

CONTENTS

SUMMARY	1	1/A5
INTRODUCTION	1	1/A5
TEST FACILITY AND PROCEDURES	2	1/A6
Facility	2	1/A6
Aircraft Suspension System	2	1/A6
Test Parameters	3	1/A7
Test Method	3	1/A7
Test Specimens	3	1/A7
Instrumentation	4	1/A8
DATA REDUCTION	5	1/A9
RESULTS AND DISCUSSION	5	1/A9
CONCLUDING REMARKS	8	1/A12
REFERENCES	10	1/A14
FIGURES	11	1/B1
APPENDIX - ACCELEROMETER DATA	37	1/C13

Item 830-H-15

NAS 1.60:1042

U.S. GOVERNMENT

NASA Technical Paper 1042

COMPLETED
ORIGINAL

Light Airplane Crash Tests
at Impact Velocities
of 13 and 27 m/sec

Emilio Alfaro-Bou and Victor L. Vaughan, Jr.

NOVEMBER 1977

NASA

55

NASA Technical Paper 1042

**Light Airplane Crash Tests
at Impact Velocities
of 13 and 27 m/sec**

Emilio Alfaro-Bou and Victor L. Vaughan, Jr.
Langley Research Center
Hampton, Virginia



National Aeronautics
and Space Administration

**Scientific and Technical
Information Office**

1977

SUMMARY

Two general aviation airplanes with a mass of 2700 kg each were crash-tested at velocities of 13 and 27 m/sec at the Langley impact dynamics research facility. These tests are the first in a program being conducted under controlled free-flight conditions to determine the effects selected impact parameters have on crash damage. In this report the only factor investigated is the effect of doubling the impact velocity. Other factors such as roll, yaw, pitch, flight path, angular rates, impact surface, fire, etc., also affect an aircraft crash but were not considered in this report.

In both tests two sequential impacts occurred: an initial impact when the fuselage nose first contacted the ground and a secondary impact when the cabin area in the vicinity of the wing spar contacted the ground. The secondary impact produced the highest accelerations in the cabin area. Doubling the impact velocity increased the normal and longitudinal peak-to-peak accelerations on the cabin floor by 52 percent. Roof normal peak-to-peak accelerations were increased by 43 percent. The occupant seats remained attached to the floor during the crash sequence and the "liveable volume" of the cabin was adequately maintained during both tests. Acceleration time history data and structural damage at various airframe locations are discussed. The test facility, instrumentation, specimen, and test method are also briefly described.

INTRODUCTION

With the rapid growth of private and commercial air traffic since World War II, increasing emphasis has been focused on the causes of passenger injuries and death in severe but potentially survivable crashes. NACA (National Advisory Committee for Aeronautics), the predecessor of NASA (National Aeronautics and Space Administration), conducted a series of full-scale aircraft crash tests with instrumented dummies in the early 1950's (refs. 1 and 2). These tests were performed by accelerating the aircraft along a horizontal guide rail into an earthen mound. Later NACA studies shed some light on the dynamic response of seat structures to impact loads (ref. 3) and resulted in a CAA (Civil Aeronautics Administration) update in static seat strength requirements. The aircraft previously tested by NACA, however, are not structurally representative of current general aviation aircraft. In 1973, a joint general aviation crash test program was initiated by the Federal Aviation Administration (FAA) and NASA.

As part of this new program, NASA Langley Research Center is conducting a series of crash tests to obtain information on aircraft crashes under controlled conditions. One objective of the program is to understand what happens inside an aircraft during a simulated crash and to learn how various crash parameters affect the magnitude and pattern of the structural damage. This information is essential for predicting structural collapse and designing new concepts for seats, occupant restraint systems, and cabin interiors. Evaluation of energy-absorbing seats and energy-absorbing floor structures is included in the joint

1

program but is not considered in this report. These energy-absorbing devices can be used to absorb and dissipate some of the impact energy to optimize the protection of the occupants. Crash test data are also to be compared with analytical predictions using finite-element elasto-plastic, large deflection, computer program predictions (ref. 4).

It is understood that there are certain lethal crashes in which the aircraft structure is damaged beyond hope of survivability for the occupants. Langley's crash studies are not directed toward such crash conditions but rather those crashes in which the impacted structure retains a "liveable volume" and has potential for occupant survivability. A "liveable volume" is a volume sufficient in size to maintain space between the occupant and the structure.

In this paper, the first two in a series of aircraft crash tests are discussed. The tests were conducted at flight-path velocities of 13 and 27 m/sec (30 and 60 mph). The effect of doubling the impact velocity is discussed in terms of structural accelerations and damage. Only the effect of velocity change is discussed in this report. Other factors affecting an aircraft crash such as roll, yaw, pitch, angular rates, flight path, various impact surfaces, fire, etc. are not covered here. These tests were not conducted to evaluate the crash safety of a particular airplane but rather to obtain data for analysis.

TEST FACILITY AND PROCEDURES

Facility

The crash tests were performed at the Langley impact dynamics research facility shown in figure 1. The gantry structure is 73 m high, 122 m long, and 81 m wide at the base. The impact surface is a reinforced concrete pad selected to provide repeatability for the tests and to allow comparison between tests conducted on the same impact surface. Shown in the figure is an airplane specimen suspended from the gantry in the ready position to be swung onto the impact surface. Detailed information on the full-scale aircraft crash facility in which the crash tests were conducted is reported in reference 5.

Aircraft Suspension System

The cable arrangement used in controlling the swing of the airplane is shown in figure 2. The airplane was suspended from the gantry by two swing cables. To each swing cable, three cables were attached at a ring junction. From each ring junction two cables were connected on the top center line of the airplane, fore and aft of the center of gravity, to control the angle of attack and the third cable was connected on the wing to support the airplane and to control roll. The interaction of all three cables was involved in yaw control. A pullback cable and harness was used to lift and hold the airplane at the desired height from which it was later released to start its downward swing. The pullback height was varied to produce impact velocities of 13 and 27 m/sec. An umbilical cable was used to transmit signals from accelerometers to a data acquisition system located in a building adjacent to the gantry.

Test Parameters

Test parameters that can be controlled at the facility are flight-path velocity, flight-path angle, angle of attack, pitch, yaw, and roll. These parameters are shown in figure 3 together with the positive direction of the aircraft coordinate system. For both tests reported herein, all parameters were nominally the same except for the flight-path velocity. In the first test the nominal flight-path velocity at impact was 13 m/sec and in the second test it was 27 m/sec. The velocity in test 2 was doubled by increasing the drop height from 9 m in the first test to 42 m.

Test Method

After preliminary checks on the aircraft impact position, pyrotechnic devices, and instrument calibration, the aircraft was pulled back to a pre-determined height to obtain the desired velocity at impact. The aircraft was then released to swing pendulum style. The cables were pyrotechnically separated from the aircraft just before impact to allow the aircraft to crash under free-flight conditions on the impact surface. At this time, the umbilical cable was still attached to the aircraft and exerted negligible restraining forces during the crash sequence. The umbilical cable was separated from its connector on the aircraft after all significant crash data had been recorded. Details of the facility capabilities, operation, suspension system, testing method, and performance are described in reference 5.

Test Specimens

Airplane specimens used for the tests were twin-engine general aviation type having a nominal mass of 2700 kg and a capacity for six to eight passengers. Both specimens, one of which is shown in figure 4, had simulated engines and tail sections which gave the proper mass distribution. The fuel bladders were filled with colored water to simulate the fuel mass and to help locate bladder leakage, if any, during the tests. Spoilers were attached to the wings to minimize the aerodynamic lift.

The exterior of the aircraft was painted yellow to enhance photographic contrast with the surroundings and black lines were painted over rivet lines to delineate the underlying structure. The interior was painted white to increase the luminosity needed by the high-speed motion-picture cameras and to increase the contrast between the dummies, seats, instruments, and structure.

The airplane specimens for both tests were similar except in the interior where in test 1, one anthropomorphic dummy was used on the first passenger seat and five lead weights were used to simulate the weight and center of gravity of the pilot, copilot, second, third, and fourth passengers.

In test 2 (fig. 4(b)) the pilot and first passenger were anthropomorphic dummies, the copilot and second passenger were manikins, and the third and fourth passengers were simulated with lead weights.

Instrumentation

The instrumentation consisted of accelerometers, high-speed cameras mounted onboard, and cameras to provide external photographic coverage of the tests.

The accelerometers used were piezoelectric type with low impedance to minimize noise over the 214-m cable lengths. The umbilical cable to the gantry was 104 m long and the cable from the gantry to the control room was 110 m in length. The signal conditioning equipment and four frequency modulated (FM) tape recorders are located in a control room. The frequency response range of the accelerometers was from 2 to 5000 Hz and signals were fed through 4- to 3300-Hz band-pass filters in the amplifiers and recorded on FM magnetic tape recorders. The maximum dynamic range of the accelerometers was $\pm 750g$. Accelerometers were installed in the left side of the specimen, symmetry of damage of impact (0° roll, 0° yaw) being assumed. They were located adjacent to the floor beam, at the base of the first passenger seat, in the dummy's pelvis and head, along the roof profile, on the tail, and on the wings and were oriented in the normal, longitudinal, and transverse directions. Each location is designated by the coordinates shown in figure 5 as follows: the accelerometer location on the floor beam nearest the nose is designated 2B9, etc. An accelerometer at that location oriented in the normal direction is designated 2B9N. Accelerometers measuring longitudinal and transverse accelerations are designated with L and T, respectively.

The piezoelectric accelerometers used in the tests exhibit various degrees of zero shift in their acceleration time histories with increasing time. This problem is compounded by the multiplicity of pulses to which each accelerometer was subjected during the tests. As a result, there is some unknown error in the absolute value of accelerations recorded after the first pulse. The first acceleration pulse and all peak-to-peak acceleration values, however, are believed to be accurate.

Three 400 pps (pictures per second) cameras were mounted onboard to photograph the areas indicated in figure 6. In test 1, one camera covered the interior structure of the nose area. A second camera covered the front of the cabin including the instrument panel and the third camera was focused on the anthropomorphic dummy in the first passenger seat. In test 2, more emphasis was placed on covering the dummies' response to the crash impact and the three interior cameras were focused on the dummies (fig. 6(b)). The aft camera also provided an overall view of the cabin interior.

Fifteen external cameras were used in both tests with framing rates of 20, 24, 400, and 2000 pps. Twelve cameras were remotely controlled and three cameras were manned to track the event. In addition, two television cameras with instant replay capabilities were used during the tests.

Actual test parameters determined from the camera coverage were flight-path, pitch, roll, and yaw angles. The cameras also recorded external and internal structural deformations, and the motions of the dummies, seats, and restraint systems. The velocities at impact were determined by radar and photographic coverage.

DATA REDUCTION

Raw data from the accelerometers contain frequencies from 4 to 3300 Hz. The least-squares fit (LSF) reduction technique was applied to the high-frequency data in an attempt to smooth the data and approximate the basic loading function at the various aircraft accelerometer locations.

A trace using this technique is shown in figure 7(a) together with the raw data trace and other traces using low pass constant amplitude, eight pole, analog filters of 60, 90, 180, and 600 Hz. An LSF trace is superimposed on the raw data for comparison. The trace is in phase with the raw data and the magnitudes of the peaks show a good average representation of the raw data. Integrations of the raw data and LSF data were made and showed that the area under both curves was the same; thus, the LSF averaging technique was validated. The LSF technique was preferred over standard filtering to avoid the inherent time lag of filtered data and provide better correlation between accelerometer data and high-speed motion-picture data.

In this report, LSF acceleration values were used throughout. The LSF technique yields acceleration values comparable with those obtained with a 150-Hz filter as may be surmised from figure 7.

RESULTS AND DISCUSSION

Nominal (planned) and actual impact parameters are tabulated in figure 3. The differences between nominal and actual values are considered acceptable. The small differences shown may be attributed to oscillations of the airplane in its flight path, catenary effects of the swing cables, wind gust velocity and direction during the tests, and other test perturbations.

Figures 8(a) and 8(b) are sequences of photographs taken during the first and second test, respectively. Time between frames is 0.05 second. The photographs clearly show the free-flight condition of the test specimen prior to initial impact. The structural damage to the fuselage occurs during two impacts: initial impact followed by a second impact. Initial impact starts when the nose first contacts the landing surface (second frame in test 1 and third frame in test 2). Second impact starts at the time the wing main spar contacts the landing surface (fifth frame). During initial impact, the floor beams in the nose yielded and caused buckling of the nose and fire wall. The combination of downward momentum of the wings and the impact of the main spar with the ground caused twisting of the main spar and loss of wing dihedral angle. For both tests, the structural damage was moderate and the cabin maintained its integrity and liveable volume.

Acceleration traces in the normal (Z-axis) direction for two extreme points on the floor beam are shown in figure 9(a). The top traces are the acceleration time histories produced by the initial impact in the nose area at point 2B9N. The trace for test 1 (solid line) shows a peak of -37g occurring 26 ms after initial ground contact whereas in test 2 (dashed line) a peak of -107g was recorded 18 ms after contact. The minus signs signify accelerations in the upward direction. ($1g = 9.806 \text{ m/sec}^2$.) After initial impact, the

specimen continues to slide forward and to rotate tail downward. The pivot point is the contact surface under the fuselage which moves aft during the downward rotation until secondary impact or slap down is completed. The crash forces are applied to the structure at the moving contact surface, which grows in area and moves rearward toward the cabin as the fuselage rotates downward.

As the specimen continues to slide forward, the cabin rotates onto the landing surface. The impact in the rear of the cabin was recorded by accelerometer 19B9N located adjacent to the floor beam. A peak-to-peak acceleration of 48g was recorded in test 1 at this location and 63g in test 2. (See fig. 9(a).) Significant accelerations recorded at the rear of the cabin (location 19B9N) do not appear until 125 ms after initial contact in test 1 and after 60 ms in test 2. Acceleration time histories adjacent to the floor beam normal to the longitudinal axis are shown in figures 9(b) and 9(c) for tests 1 and 2, respectively. From top to bottom the traces represent nose to tail accelerometer locations. The higher acceleration peaks of each trace occurred when that location on the floor beam was over the fuselage-ground contact point. Zero time represents initial contact. In test 2 (fig. 9(c)) at twice the impact velocity of test 1, the accelerations were higher and the elapsed time for significant accelerations was of shorter duration.

A complete set of the acceleration time history traces for the the specimen in each test are included in the appendix. They are presented in plots according to their location and orientation. The locations are divided into the floor beam, cabin floor and wing, roof, and dummies.

Photographs showing external damage to the specimens for tests 1 and 2 are shown in figures 10 and 11, respectively. The damage to the nose area of the specimen was approximately the same for both tests. (See figs. 10(a) and 11(a).) The crash forces in the nose area were more intense and the damage more severe than in other parts of the specimen. However, the damage was restricted to the cowling and fire wall where most of the impact energy was absorbed by crushing of the structure during nose contact. Some of the remaining energy in the form of small attenuated forces and motions was transmitted to the cabin area.

In test 2 the skin wrinkled from nose to tail on both sides of the fuselage. The overlapping sheet metal on top of the fuselage separated along the rivet line behind the first window due to rivet shear. Similar breaks occurred along the rivet line at the base of the windows. (See figs. 11(a) and 11(b).) The separation along the rivet line on top and along the side of the fuselage occurred during second impact when the roof continued to move downward as the floor was brought to rest and this movement caused a lateral expansion of the cabin.

The interior damage to the cabin in test 1 was relatively mild, significant damage occurring in the fore cabin in the vicinity of the instrument panel and fire wall. The damage to the cabin interior for test 2 is shown in figures 11(c) and 11(d). In test 2 the cross members in the floor structure under the front legs of the pilot and copilot seats collapsed. This was due to the forward and downward thrust of the seats and occupants. In the cabin area aft of the main spar (fig. 11(c)), the structural damage is evident in the deflection of the two outer floor panels about the floor beams. During second impact, the rounded

bottom portion of the fuselage beneath the floor beams contacts the ground and is flattened. As the impact progresses, the vertical motion of the floor beams is arrested while the roof and sides of the cabin continue to move downward. This downward movement of the sidewalls causes the two floor beams to appear to move upward and outward. This deformation pattern continues until the impact energy is dissipated in deforming the cabin structure. At maximum cabin deformation the support frames yielded on their sides and the cabin assumed an oval shape (fig. 11(d)). In test 2, at maximum cabin deformation the sides of the airplane moved outward 21 cm at the center and the distance between the roof and the floor was reduced by 23 cm. Figure 12 presents peak-to-peak normal and longitudinal accelerations at longitudinal stations along the specimen structure. Peak-to-peak accelerations measured normal to the floor beam for tests 1 and 2 are shown in figure 12(a). They give a general idea of the acceleration levels at various locations adjacent to the floor beams. The average peak-to-peak acceleration was 78 percent higher in test 2 than in test 1. For both tests, the accelerations were higher at the nose and near the main spar, and lower at the fire wall and toward the rear of the cabin.

The average values of the longitudinal peak-to-peak accelerations at locations adjacent to the floor beam are shown in figure 12(b) and were approximately 40 percent lower than the normal acceleration value in corresponding locations for test 1 and 57 percent lower for test 2. In test 1 the peak-to-peak longitudinal values were higher near the main spar and correspond to high normal acceleration values at the same location. In test 2, the average value of longitudinal peak-to-peak accelerations was 26 percent higher than in test 1.

The peak-to-peak accelerations normal to the roof were higher in the nose area. Average values were 43 percent higher in test 2 than in test 1 and are shown in figure 12(c). Figures 12(d) and 12(e) show the peak-to-peak accelerations on the cabin floor in the normal and longitudinal directions, respectively. In test 2 both the normal and longitudinal peak-to-peak accelerations were approximately 52 percent higher than in test 1.

The peak-to-peak normal accelerations on the roof (location 14G9N, fig. 12(c)) and adjacent to the floor beam (location 15B9N, fig. 12(a)) are 36g and 85g, respectively, for test 1 and 80g and 150g for test 2. In this comparison, the roof accelerations are 58 percent lower than those at the floor beam for test 1 and 47 percent lower for test 2. The lower roof accelerations reflect the effect of fuselage shell deformations and load alleviation as discussed for figure 11. After the impact was over, the cabin structure returned approximately to its original shape, but the floor beams remained deformed. In this test the apparent floor beam protrusion resulted in a slight rotation of the seats toward their respective side windows as shown in figure 11(d).

Figure 13 is a plot of the normal accelerations on the floor at the base of the first passenger seat. The time of main spar contact with the ground was determined photographically and is superimposed on the traces for reference. In test 1 (fig. 13(a)) and in test 2 (fig. 13(b)) the combined effect of structural deformation, angular acceleration, and timing produces higher peak-to-peak accelerations on the cabin floor at the front seat legs compared with the accelerations at the rear seat legs. Also during second impact the peak-to-peak accelerations on the floor were higher on the aisle side than those on the

window side. This was due to the larger displacements on the window side because of the shell geometry. The average of the peak-to-peak accelerations at the four seat legs in test 2 was 78 percent higher than the average in test 1. Peak-to-peak values are used because of unknown errors in the absolute value of accelerations, measured by the piezoelectric accelerometers, after the first acceleration pulse. The seats remained attached to the floor during both tests.

In test 2, the peak-to-peak acceleration at the dummy pelvis along the spine was 76g (fig. 13(b)). In test 1 the dummy pelvis was not instrumented. Although a direct comparison between normal peak-to-peak accelerations on the floor and on the dummy pelvis could not be made because the orientation of the accelerometer along the spine changed with dummy motions during the test, it appears that some energy dissipation or force alleviation has taken place due to seat deformation. The front seat legs are experiencing peak-to-peak normal accelerations of 97g and 105g. (The rear seat legs are averaging closer to normal peak-to-peak accelerations of 72g.)

CONCLUDING REMARKS

Two similar general aviation airplane test specimens were crash tested at the Langley impact dynamics research facility at speeds of 13 and 27 m/sec. With the exception of impact velocity, all parameters were essentially the same for both tests. In both tests two types of sequential impacts occurred: an initial impact when the fuselage nose first contacted the ground and a second impact when the cabin area in the vicinity of the wing main spar contacted the ground. After second impact the specimens continued to skid horizontally until they came to a stop.

Accelerations in the cabin due to initial impact were minimal, as most of the energy from initial impact was absorbed during crushing of the fuselage nose structure. The second impact produced the highest accelerations in the cabin area.

The average peak-to-peak acceleration on the cabin floor in the normal and in the longitudinal directions was approximately 52 percent higher in test 2 than in test 1. The average peak-to-peak acceleration normal to the floor at the base of the first passenger seat was 78 percent higher in test 2. In both tests the seats remained attached to the floor during the crash sequence.

In test 2 the average peak-to-peak acceleration adjacent to the floor beam was 78 percent higher in the normal direction and 26 percent higher in the longitudinal direction than in test 1. The average peak-to-peak longitudinal acceleration was 40 percent lower in test 1 than the average normal peak-to-peak acceleration at corresponding locations and 57 percent lower in test 2.

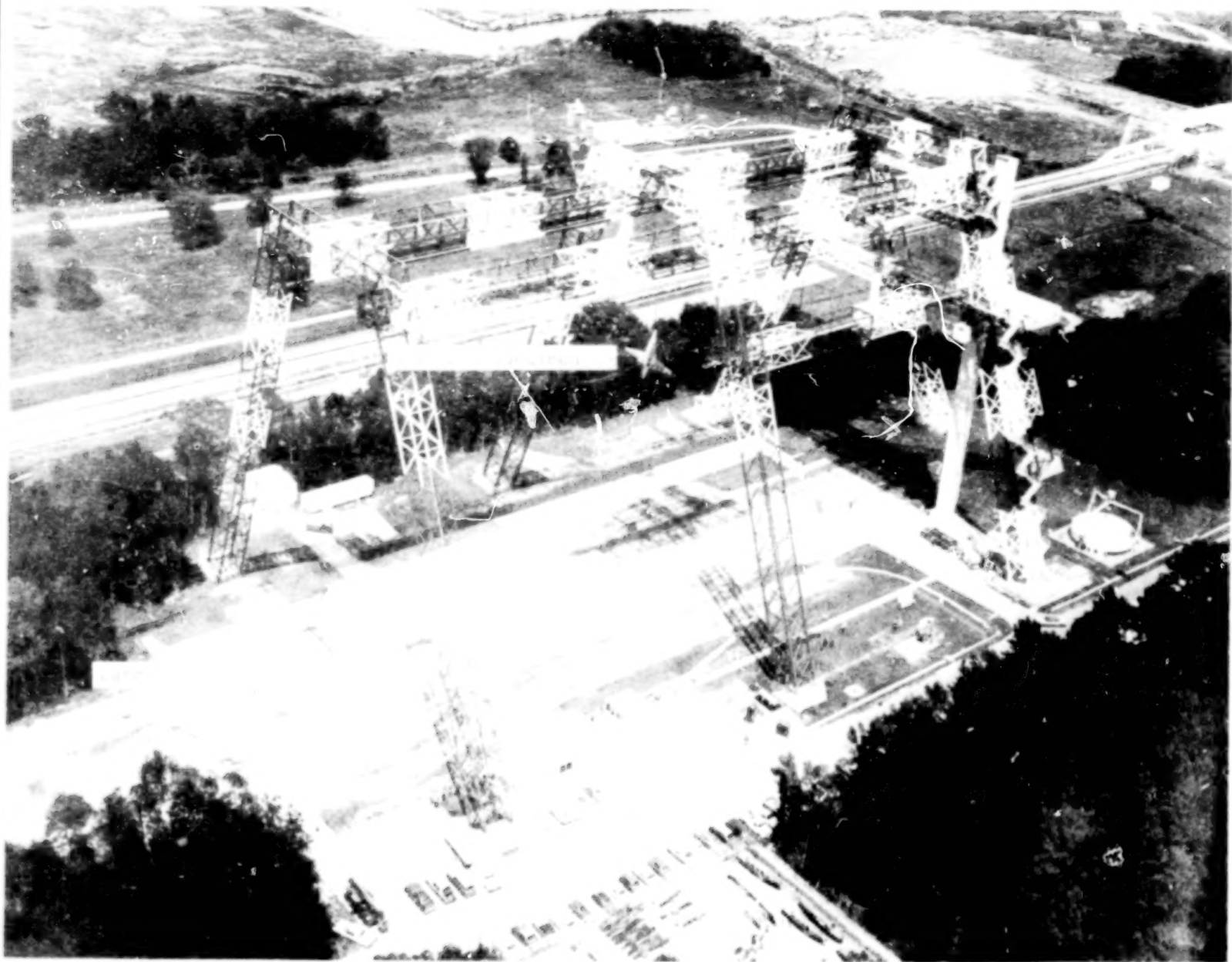
The average peak-to-peak normal acceleration at the roof was 43 percent higher for test 2 than for test 1. A comparison of peak-to-peak accelerations in the cabin at a location on the roof over the main spar and at a location adjacent to the floor beam (also behind the main spar) shows that the roof acceleration was 58 percent lower in test 1 and 47 percent lower in test 2.

The "liveable volume" of the cabin was adequately maintained throughout both tests.

Langley Research Center
National Aeronautics and Space Administration
Hampton, VA 23665
August 31, 1977

REFERENCES

1. Preston, G. Merritt; and Mosen, Jacob C.: Crash Loads. NACA Conference on Airplane Crash-Impact Loads, Crash Injuries and Principles of Seat Design for Crash Worthiness (Cleveland, Ohio), Apr. 1956, pp. 2-1 - 2-47.
2. Eiband, A. Martin; Simpkinson, Scott H.; and Black, Dugald O.: Accelerations and Passenger Harness Loads Measured in Full-Scale Light-Airplane Crashes. NACA TN 2991, 1953.
3. Pinkel, I. Irving; and Rosenberg, Edmund G.: Seat Design for Crash Worthiness. NACA Rep. 1332, 1957.
4. Alfaro-Bou, E.; Hayduk, R. J.; Thomson, R. G.; and Vaughan, V. L., Jr.: Simulation of Aircraft Crash and Its Validation. Aircraft Crashworthiness, Kenneth Saczalski, George T. Singley III, Walter D. Pilkey, and Ronald L. Huston, eds., Univ. Press of Virginia, c.1975, pp. 485-497.
5. Vaughan, Victor L., Jr.; and Alfaro-Bou, Emilio: Impact Dynamics Research Facility for Full-Scale Aircraft Crash Testing. NASA TN D-8179, 1976.



L-74-2505.3

Figure 1.- Langley impact dynamics research facility.

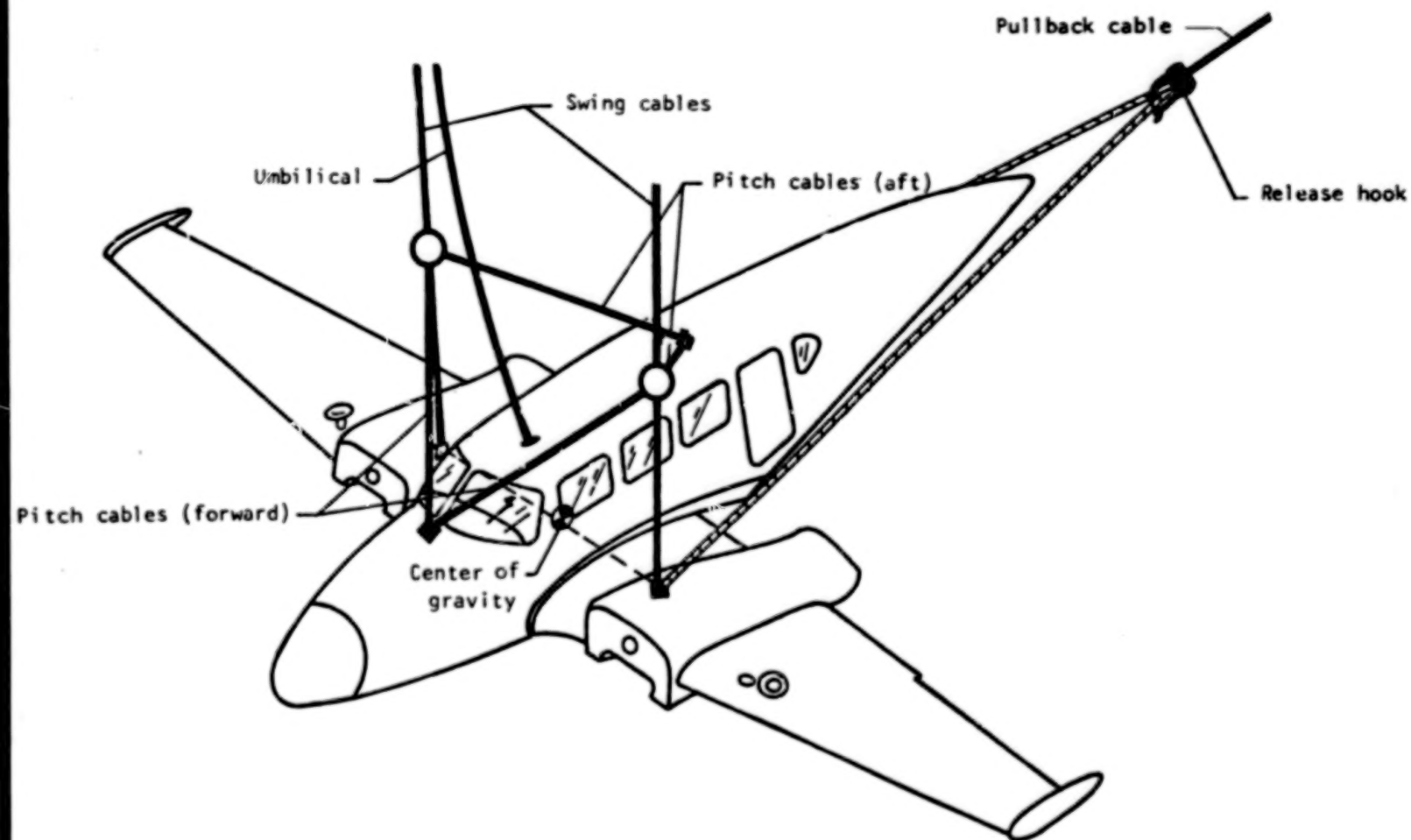


Figure 2.- Suspension system.

Test parameter	Nominal	Actual	
		Test 1	Test 2
Flight-path angle, γ	-15°	-17°	-16°
Angle of attack, α	0°	1°	4°
Pitch angle, θ	-15°	-16°	-12°
Roll angle, ϕ	0°	0°	0°
Yaw angle, ψ	0°	0°	2°
Flight-path velocity, test 1, V_1	13 m/s	13 m/s	-
Flight-path velocity, test 2, V_2	27 m/s	-	27 m/s

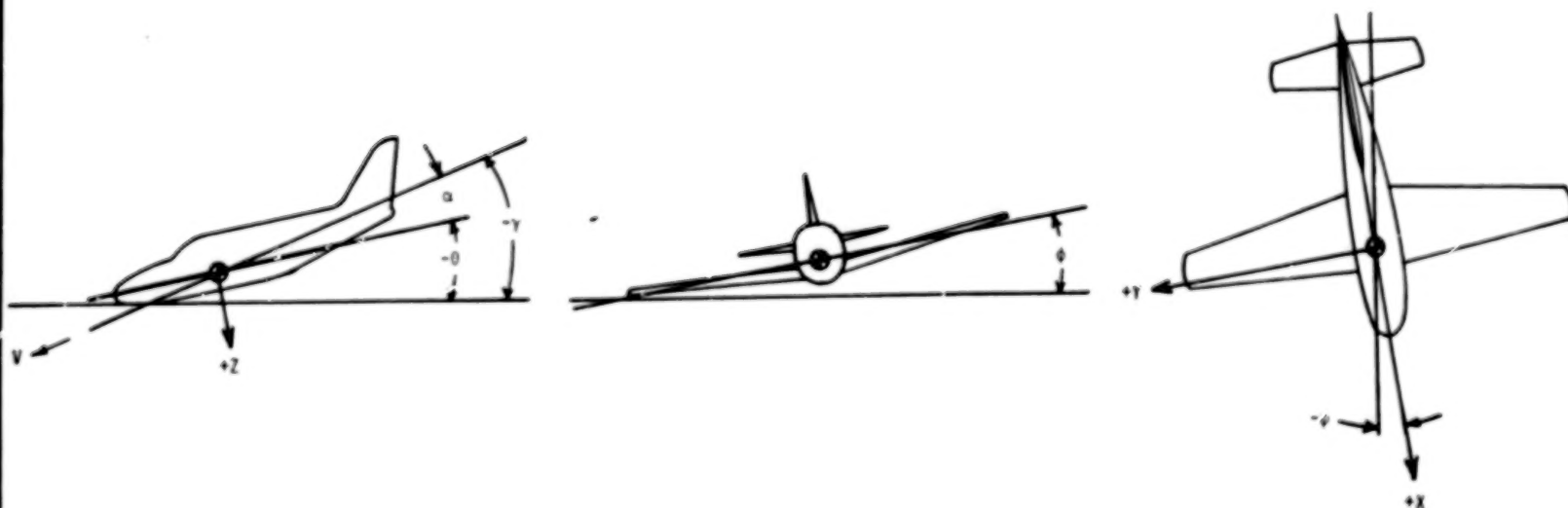


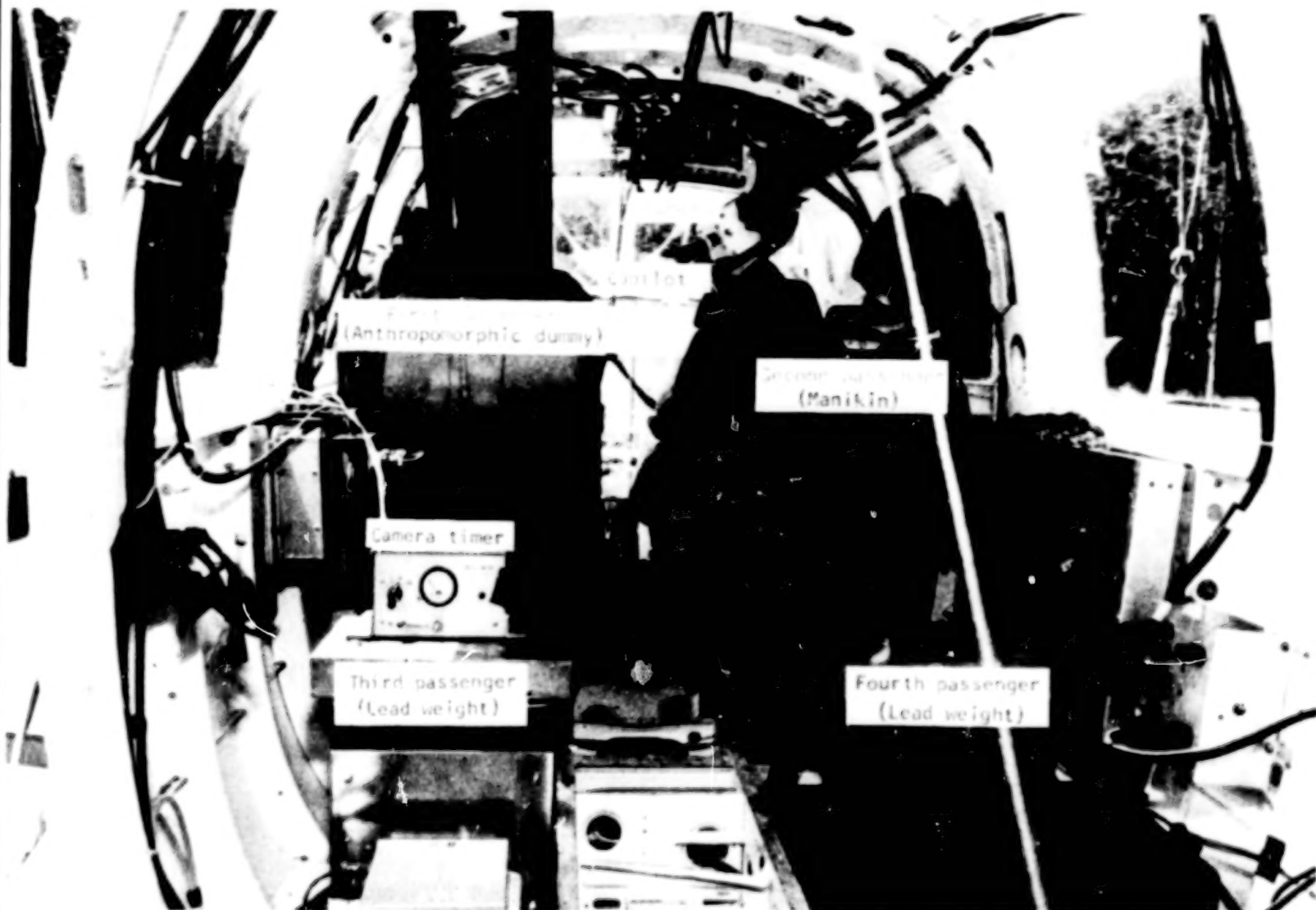
Figure 3.- Geometric crash test parameters.



(a) Exterior view.

L-74-2648.1

Figure 4.- Airplane specimen, test 2.



L-74-2653.1

(b) Interior view.

Figure 4.- Concluded.

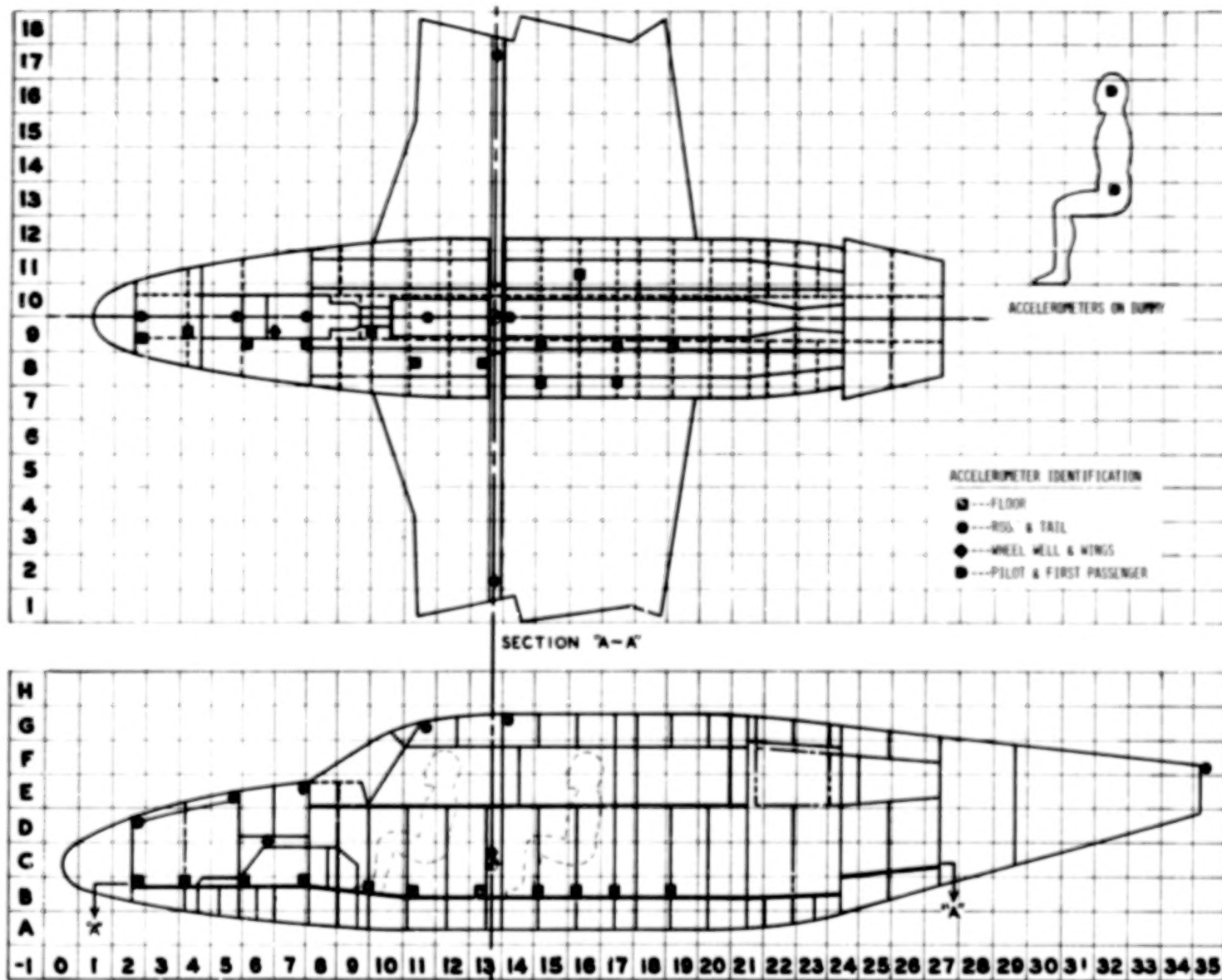
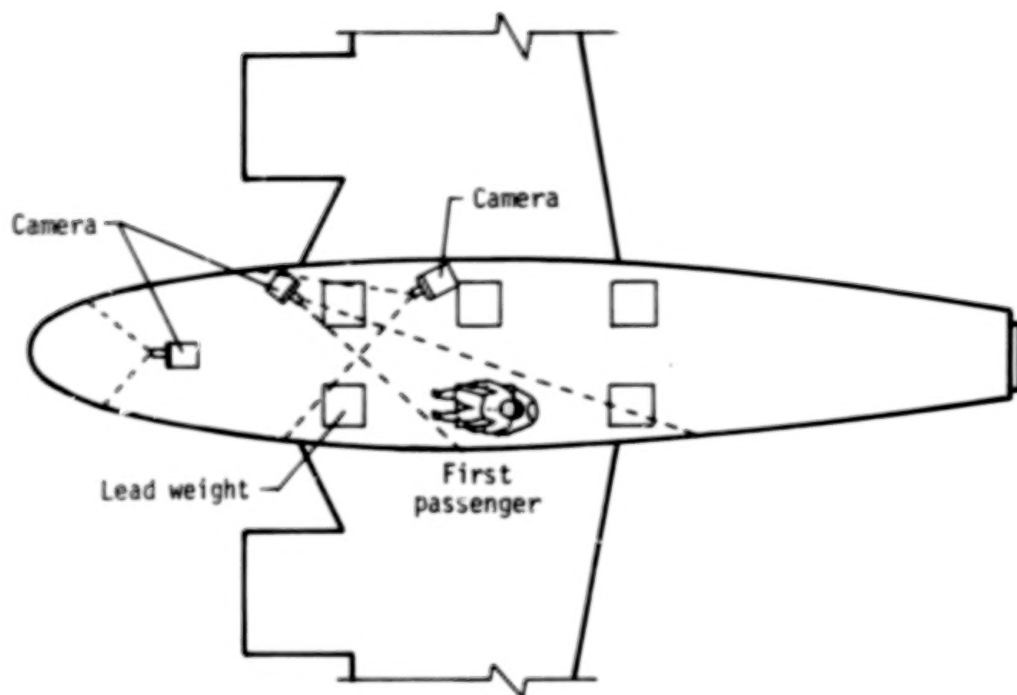
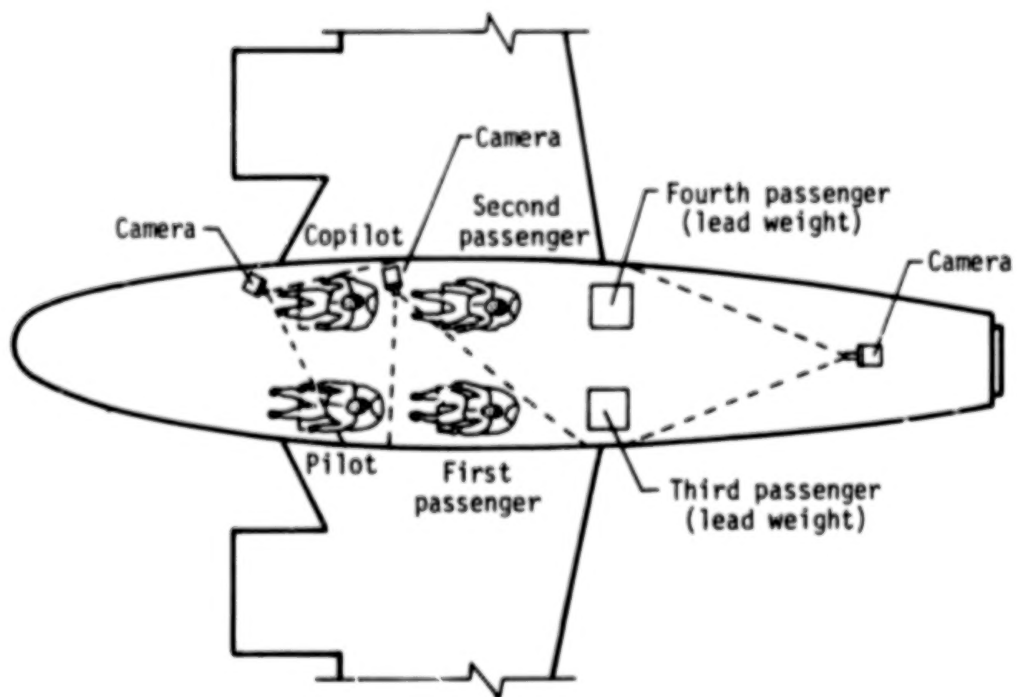


Figure 5.- Accelerometers on board aircraft.



(a) Camera arrangement in test 1.



(b) Camera arrangement in test 2.

Figure 6.- Onboard camera location.

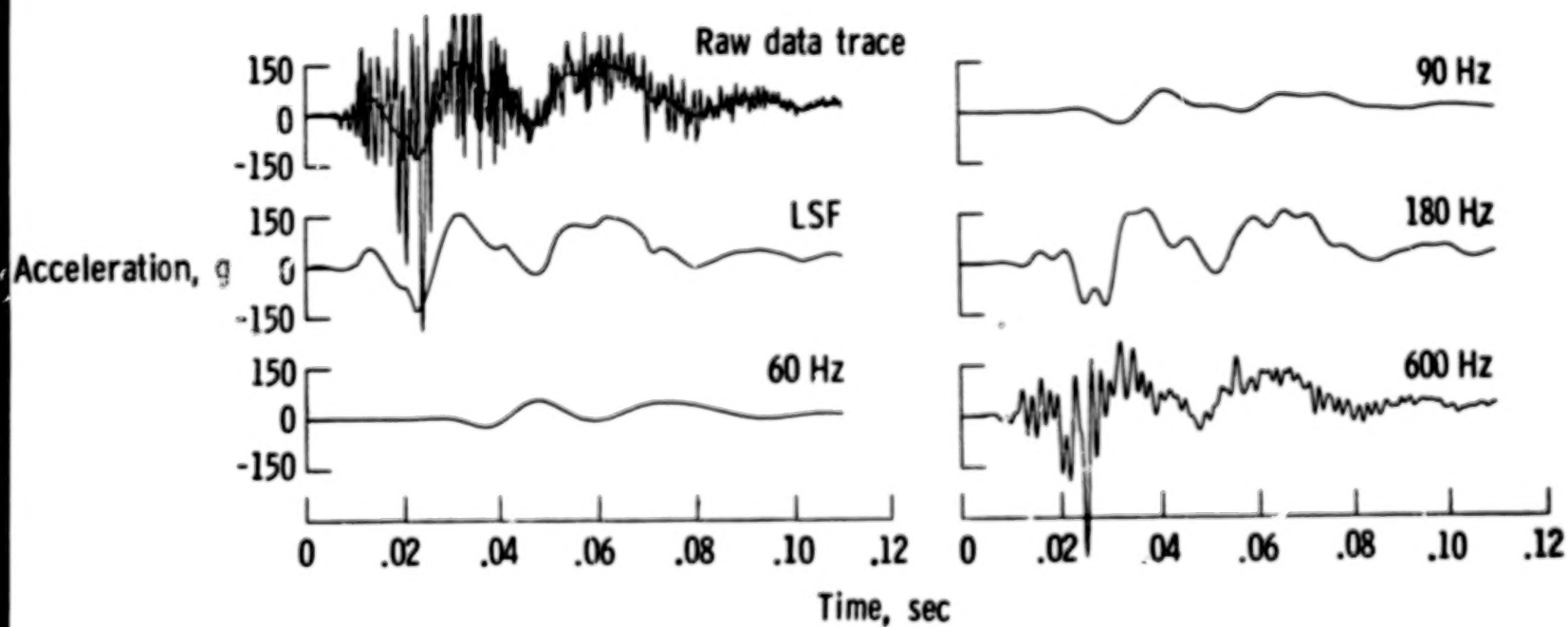


Figure 7.- Data reduction. Filtering effects on data from accelerometer 2B9N. Test 2.



Before impact



Initial impact, $t = 0$



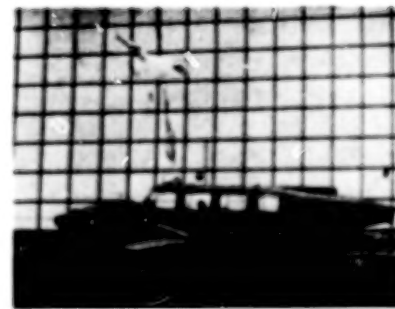
$t = 0.05$ s



$t = 0.10$ s



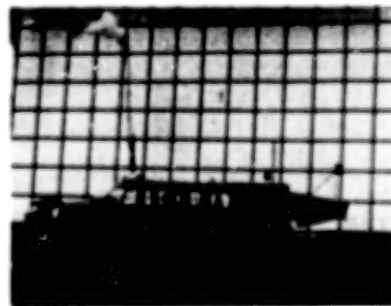
$t = 0.15$ s



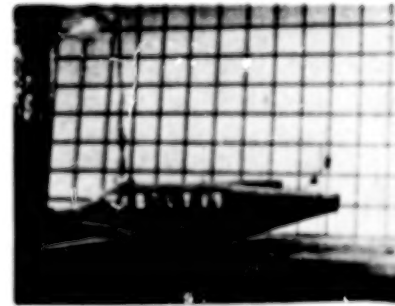
$t = 0.20$ s



$t = 0.25$ s



$t = 0.30$ s

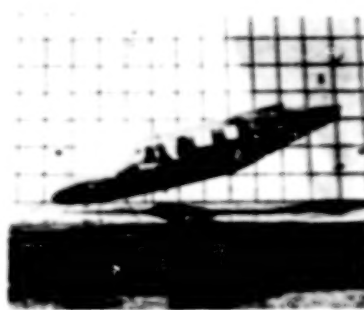
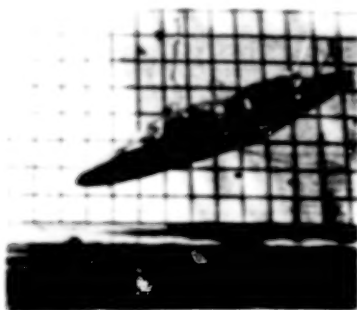


$t = 0.35$ s

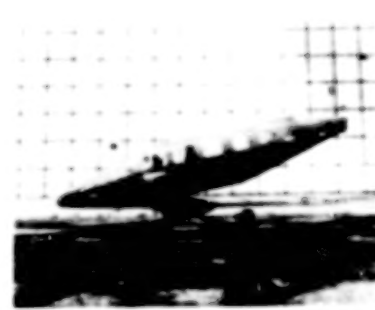
L-74-1645.1

(a) Test 1.

Figure 8.- Photographic sequence of crash test.



Before impact



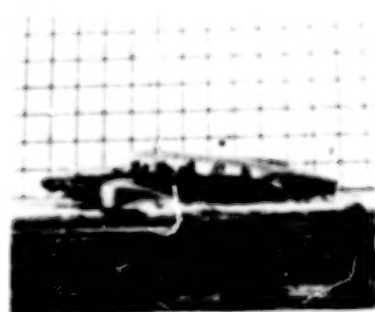
Initial impact, $t = 0$



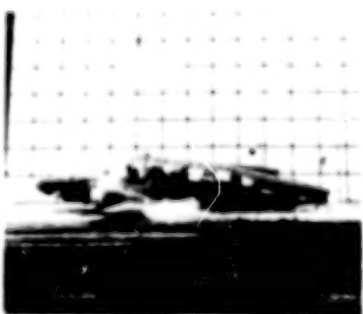
$t = 0.05 \text{ s}$



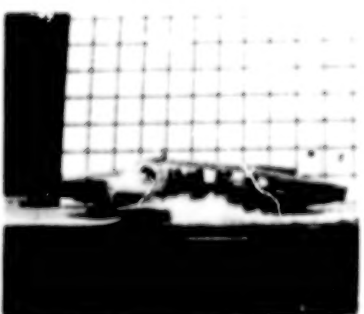
$t = 0.10 \text{ s}$



$t = 0.15 \text{ s}$



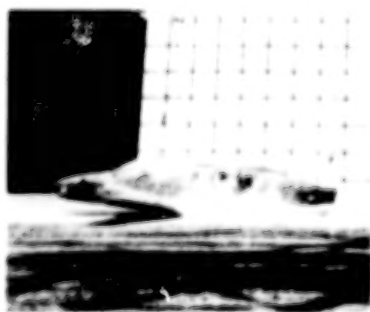
$t = 0.20 \text{ s}$



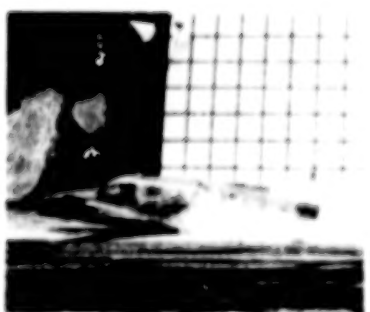
$t = 0.25 \text{ s}$



$t = 0.30 \text{ s}$



$t = 0.35 \text{ s}$



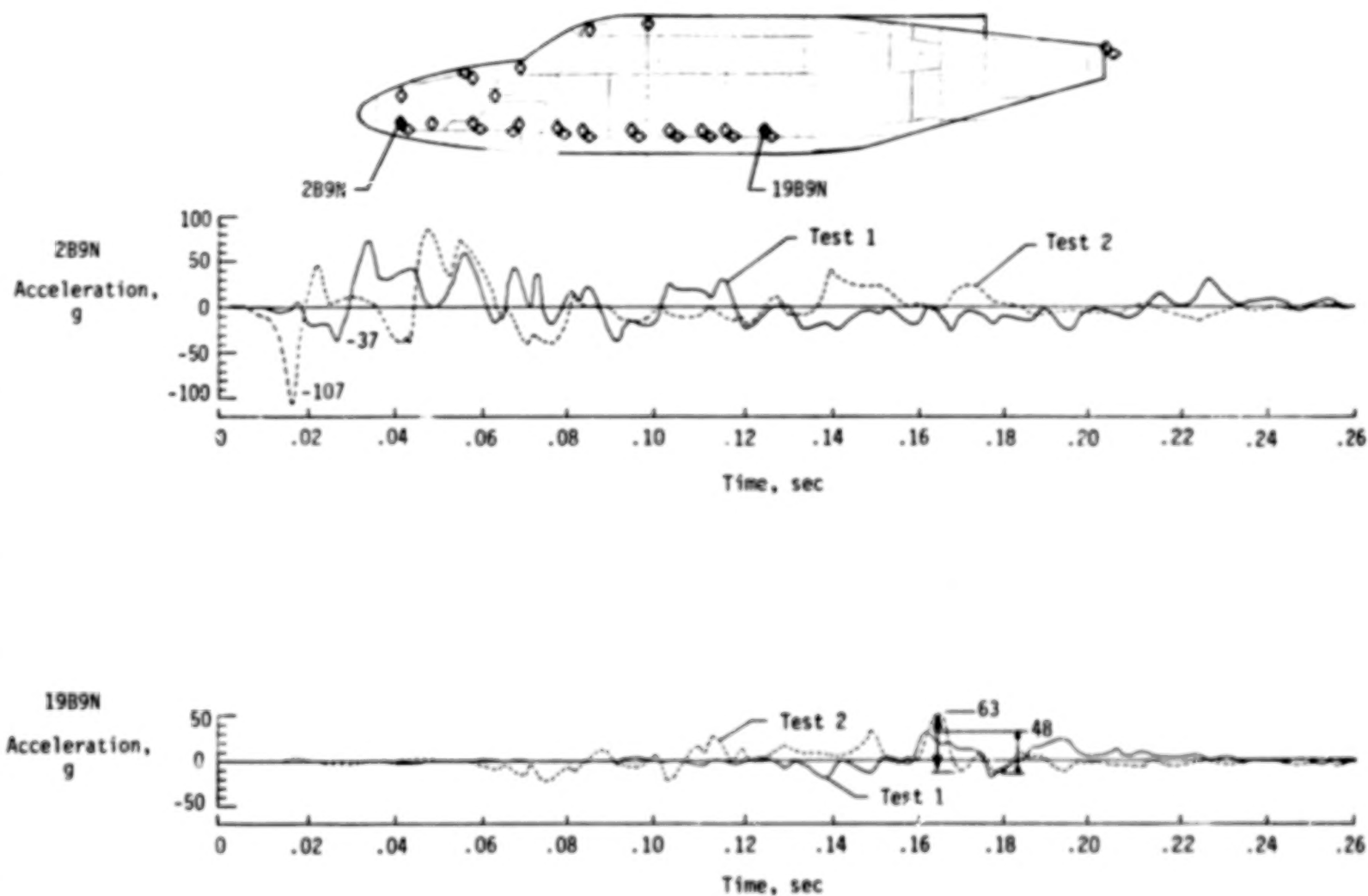
$t = 0.40 \text{ s}$



$t = 0.45 \text{ s}$

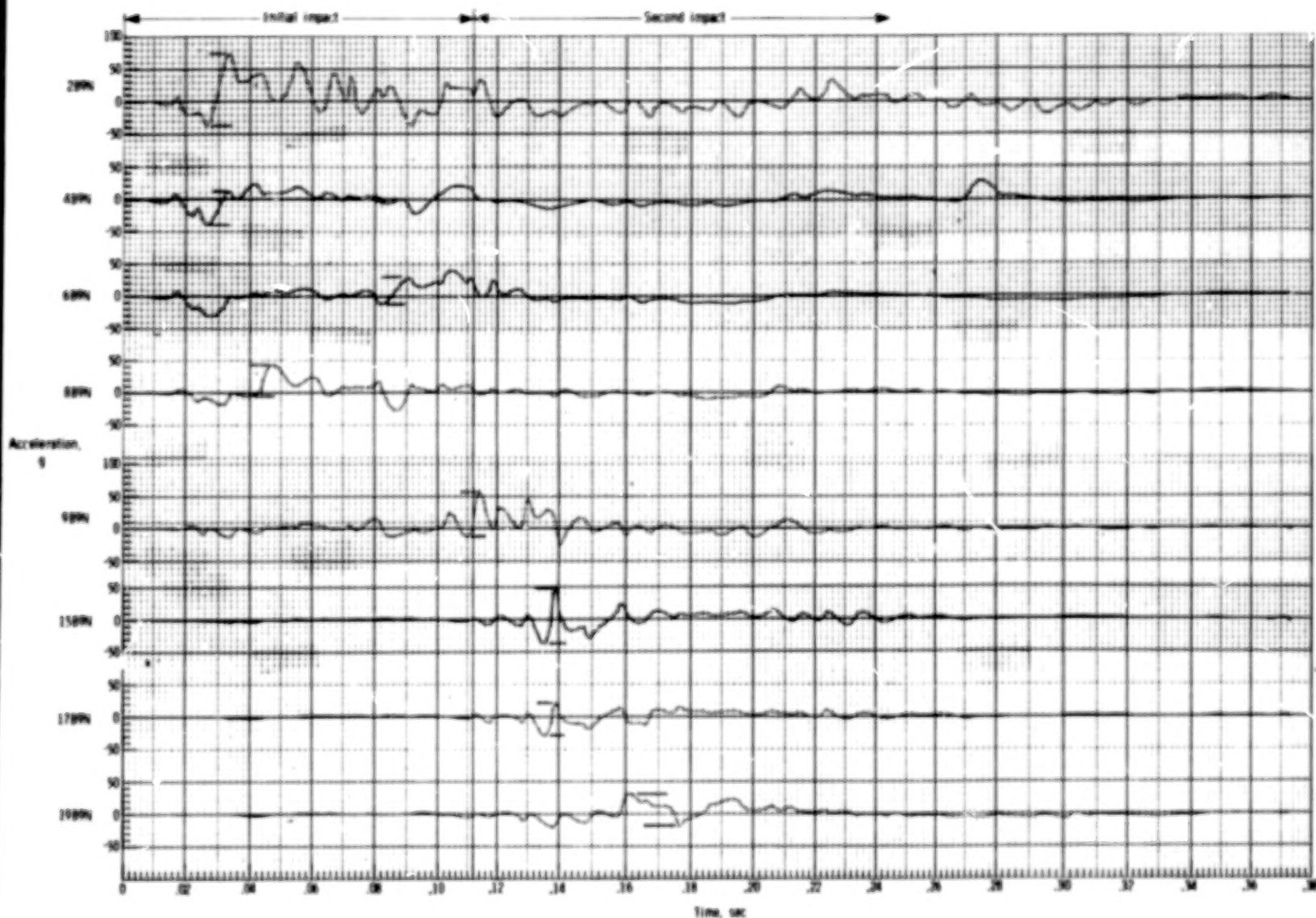
(b) Test 2.

L-74-2819.1



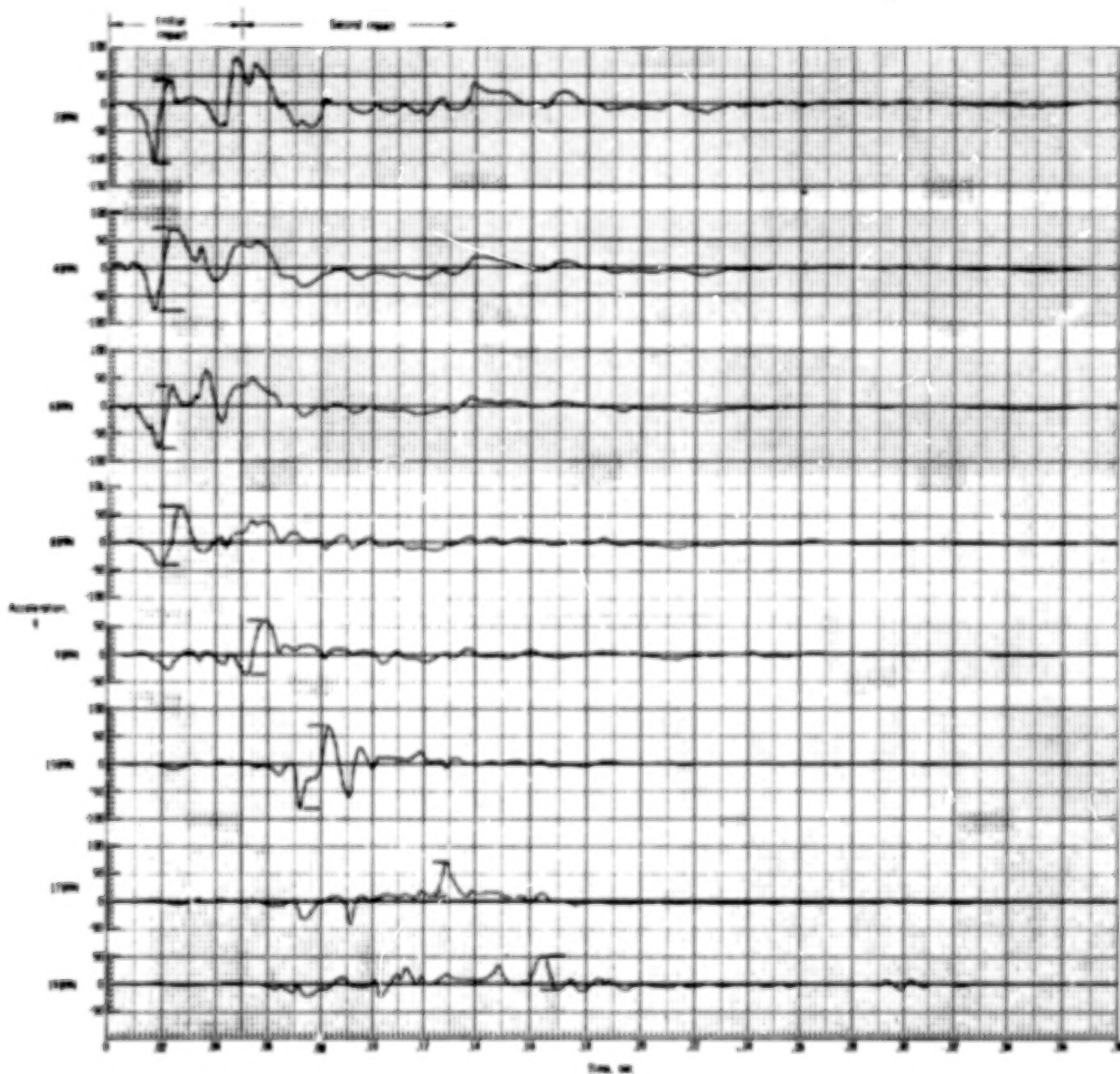
(a) Accelerations at two extreme points.

Figure 9.- Normal (Z-axis) LSP acceleration traces adjacent to floor beam.



(b) Accelerations in sequence from fore to aft. Test 1.

Figure 9.- Continued.



(c) Accelerations in sequence from fore to aft. Test 2.

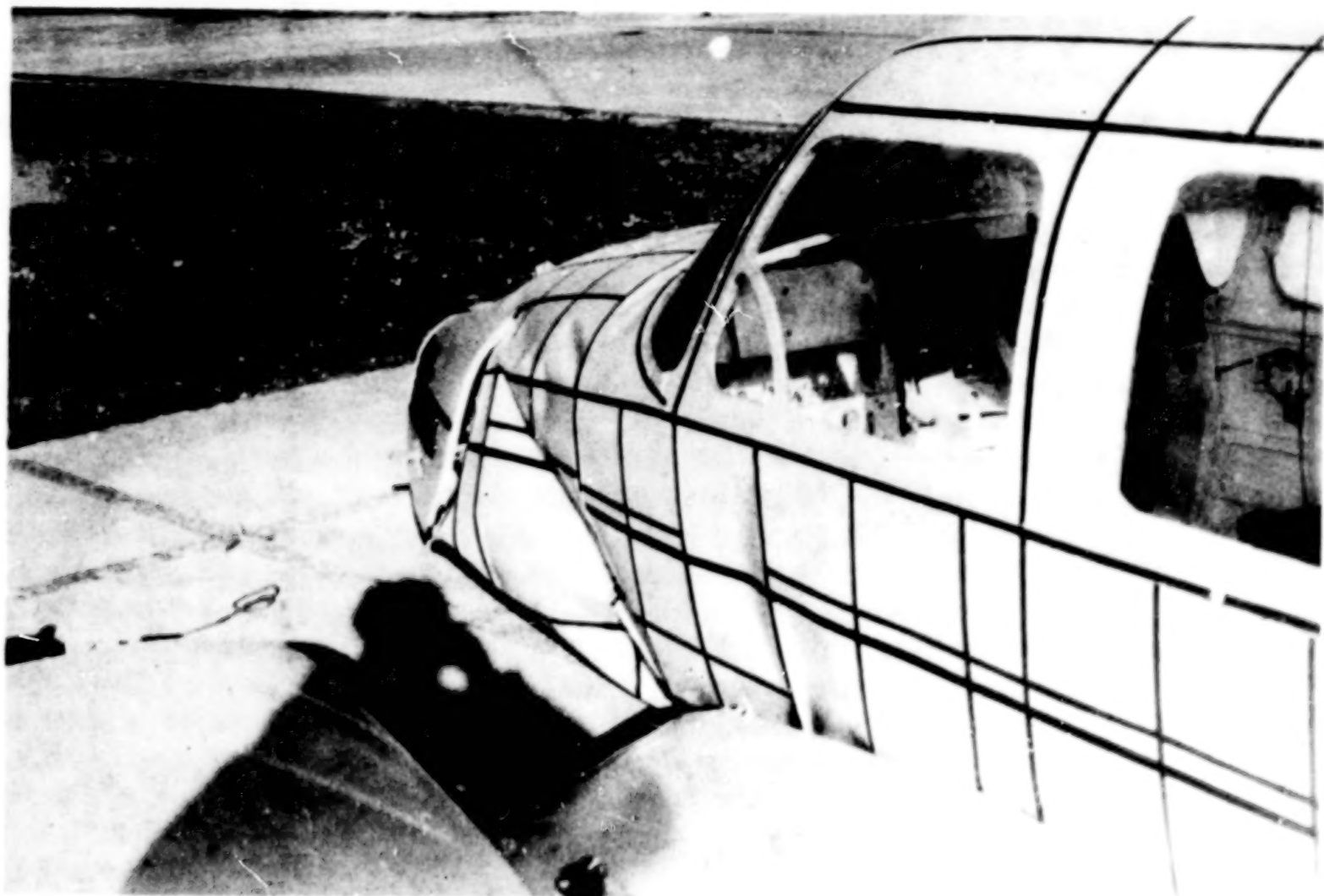
Figure 9.- Concluded.



L-74-1579

(a) Overall damage.

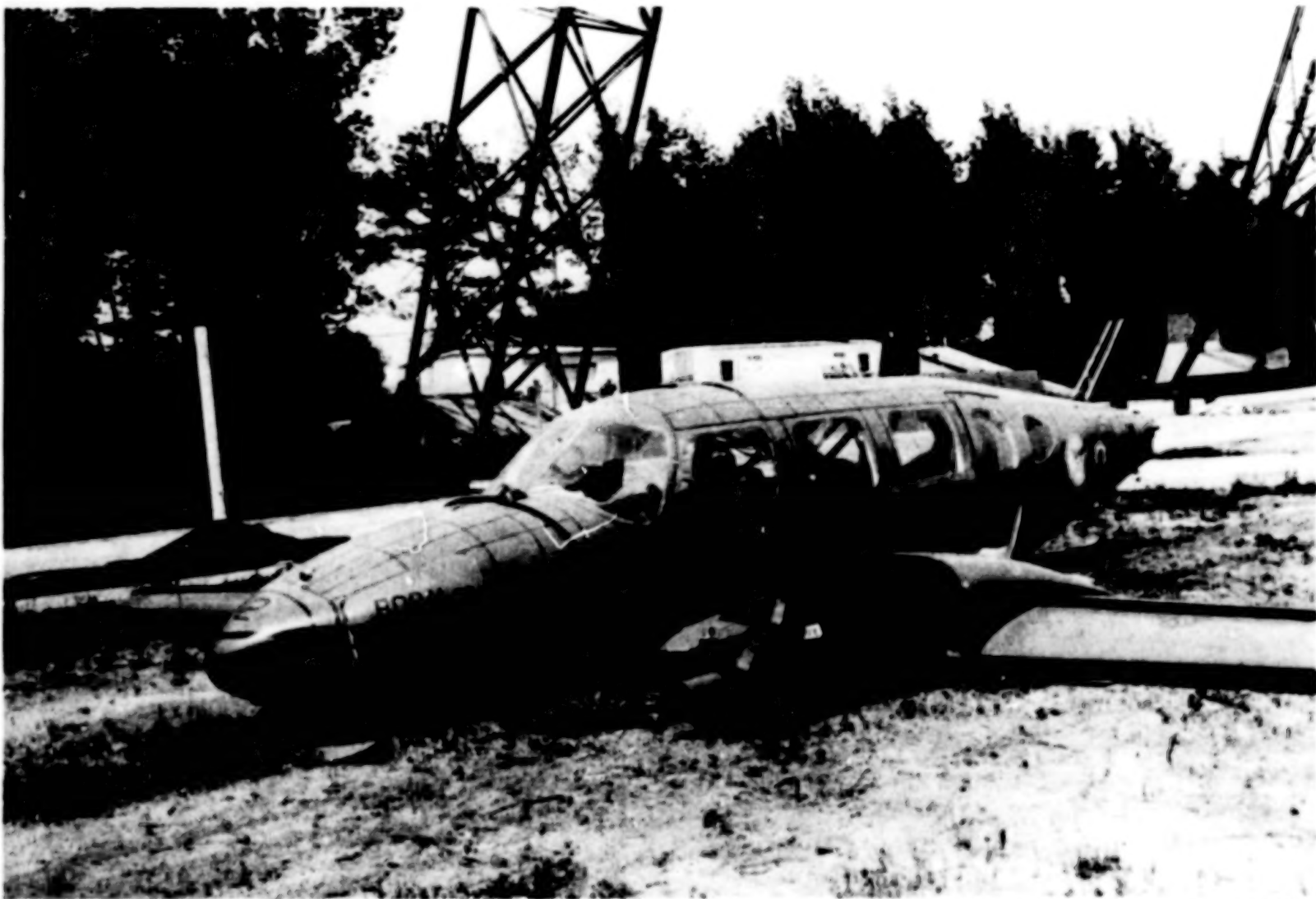
Figure 10.- Exterior damage in test 1.



(b) Closeup of nose damage.

L-74-724

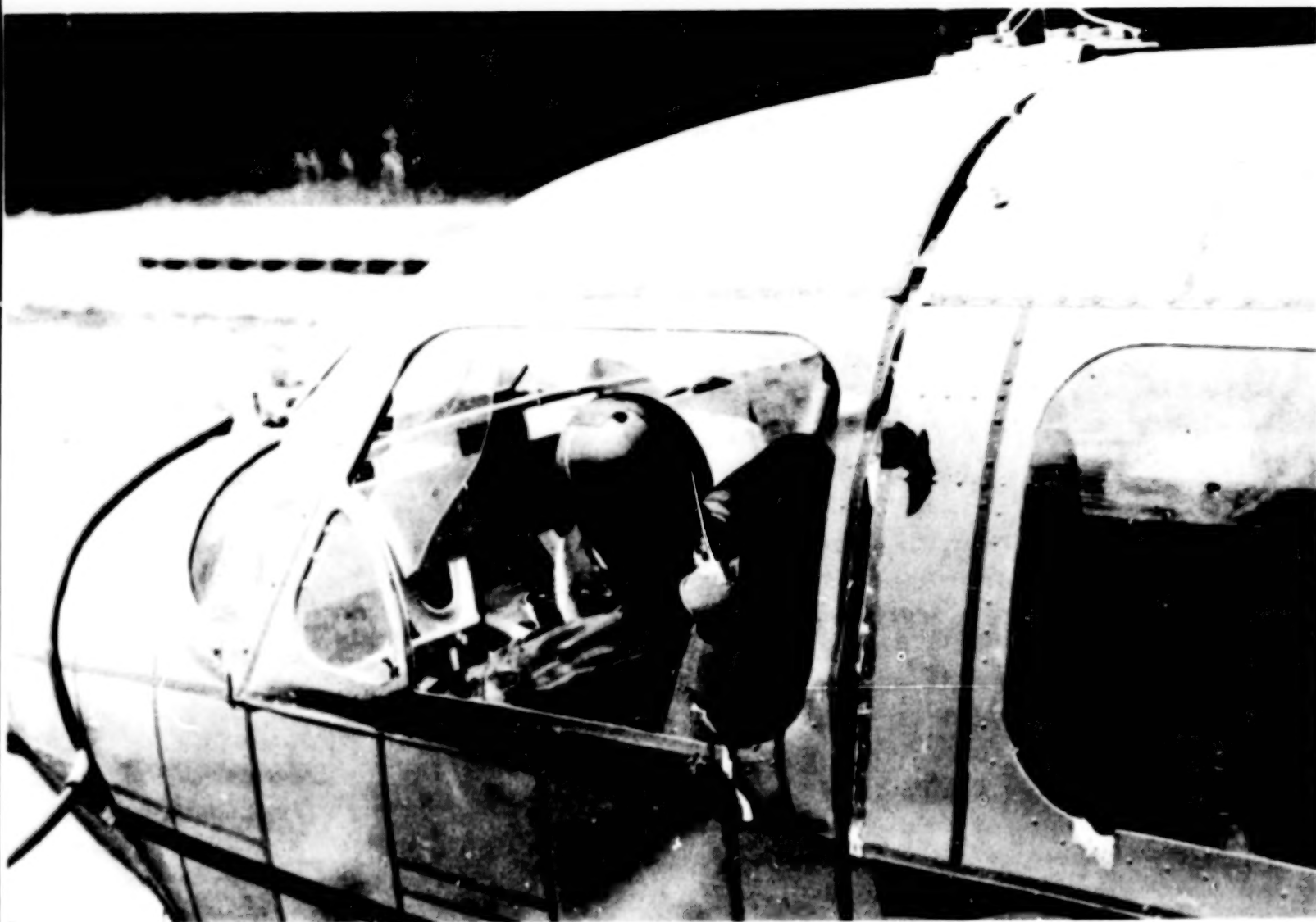
Figure 10.- Concluded.



L-74-2629

(a) Overall exterior damage.

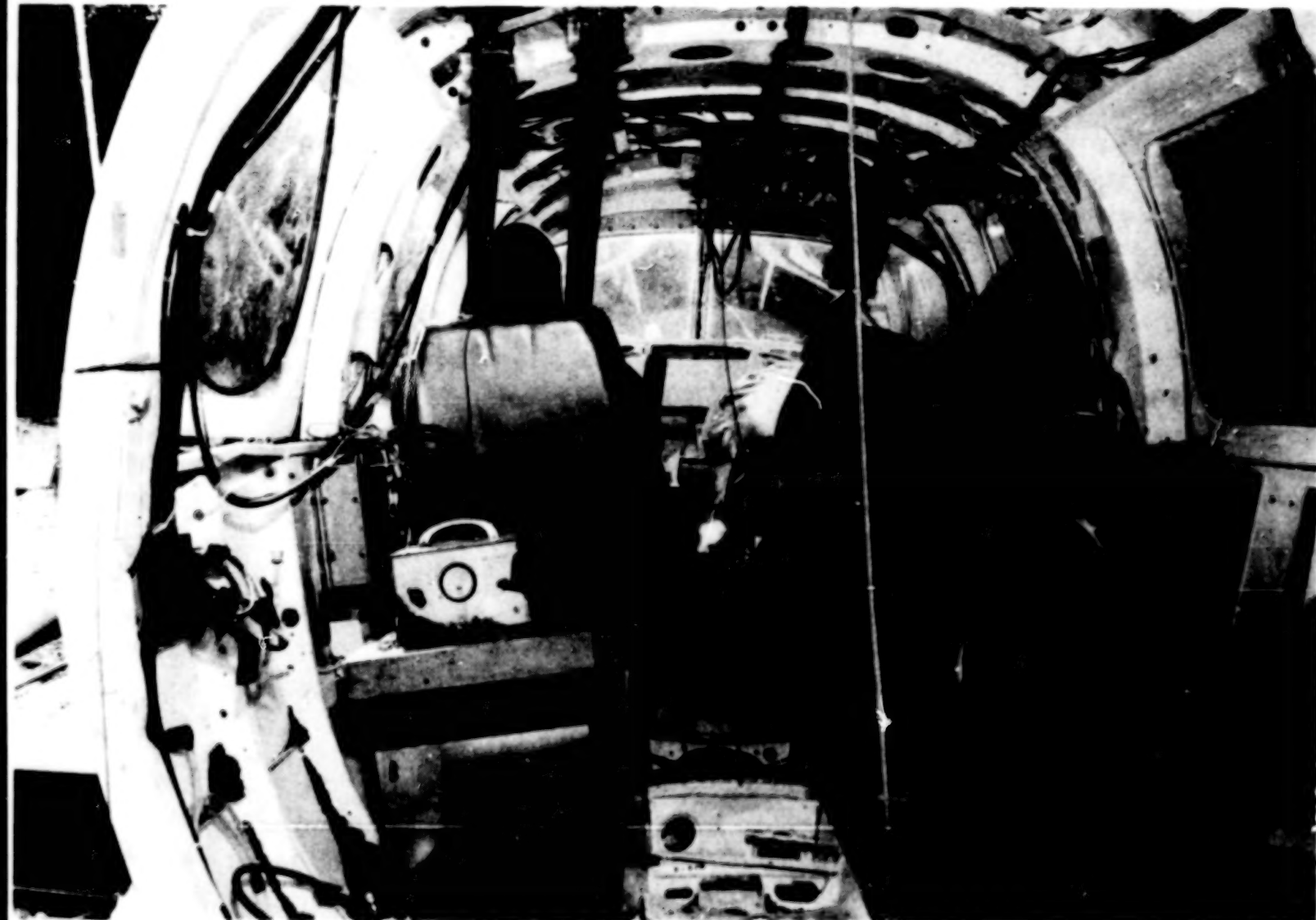
Figure 11.- Airplane damage in test 2.



L-74-2632

(b) Sheet metal separation along rivet lines.

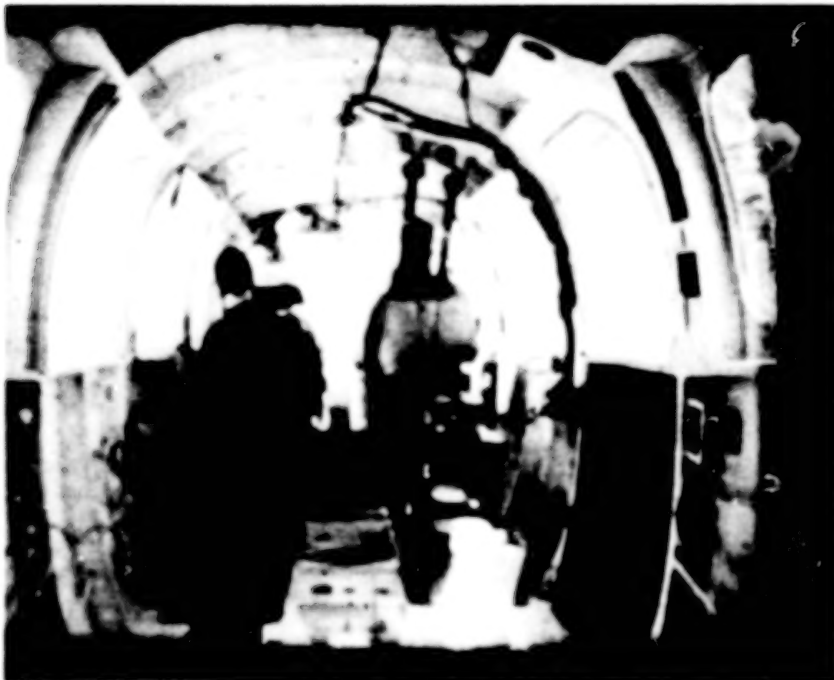
Figure 11.- Continued.



L-74-2642

(c) Interior damage.

Figure 11.- Continued.



Before impact

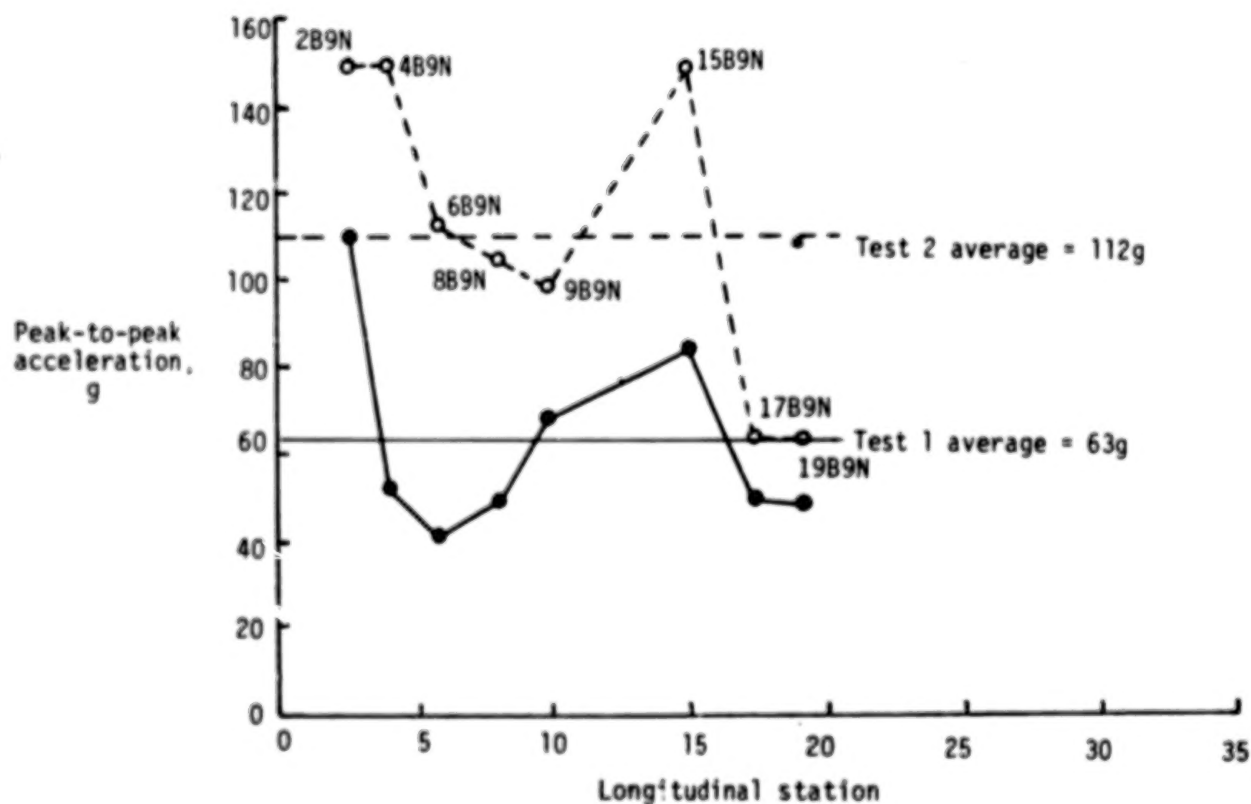
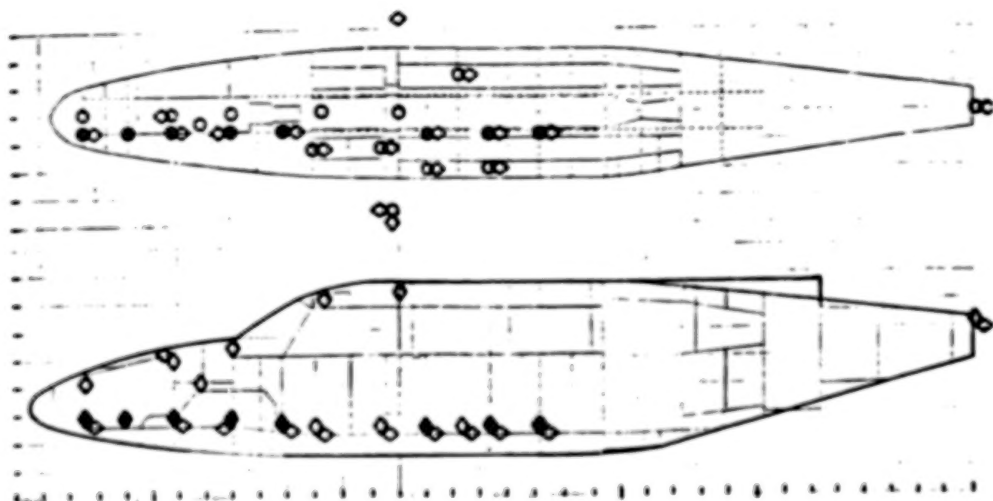


During impact

L-77-276

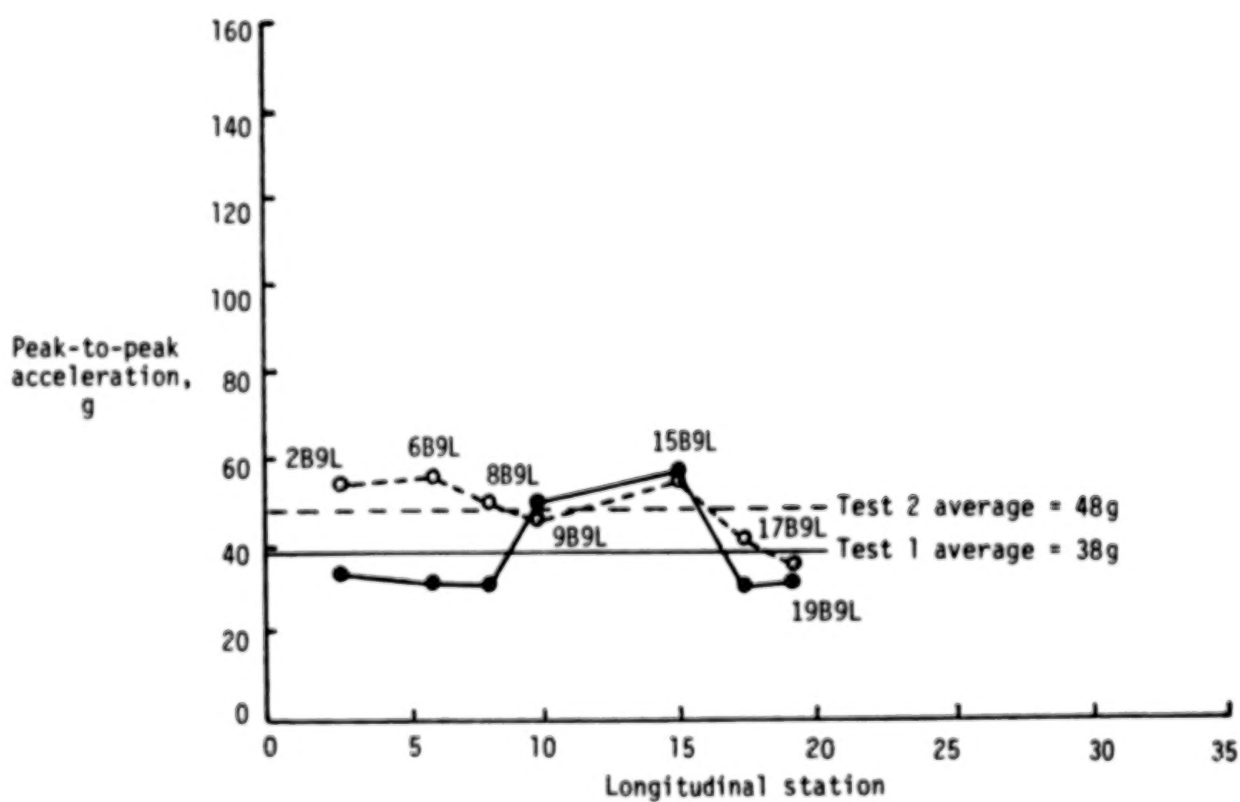
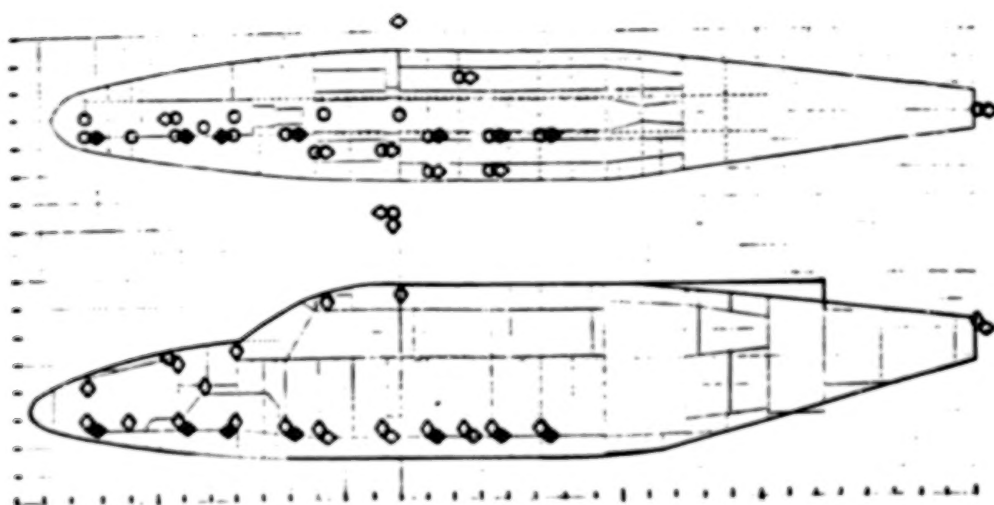
(d) Maximum cabin deformation during impact.

Figure 11.- Concluded.



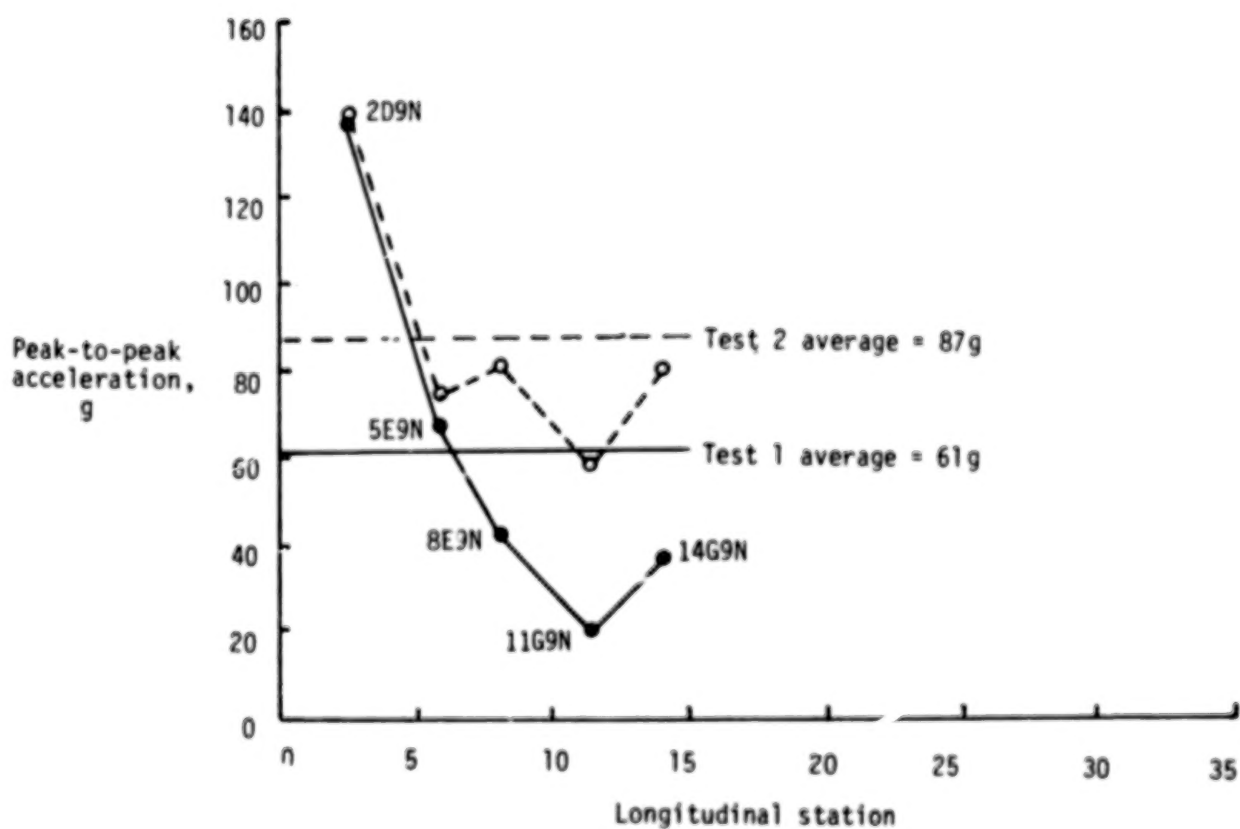
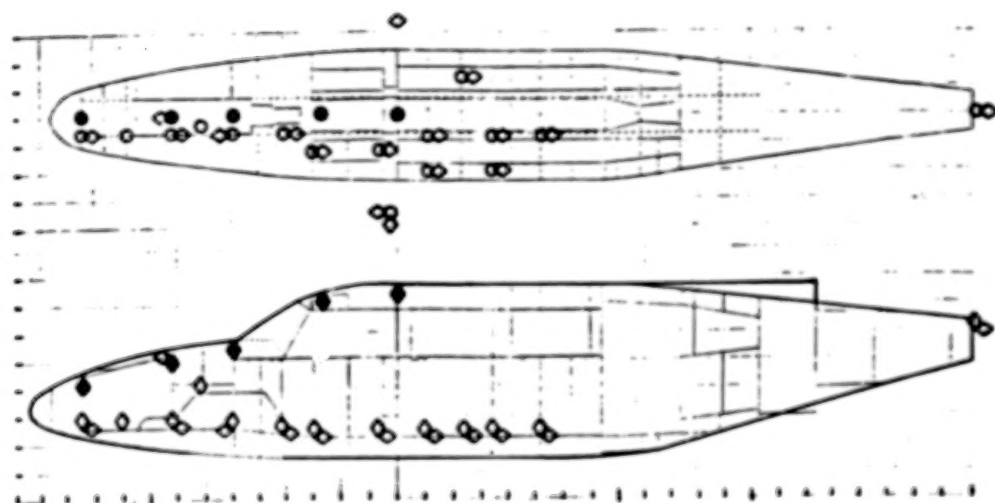
(a) Normal accelerations adjacent to floor beam.

Figure 12.- Peak-to-peak accelerations on structure.



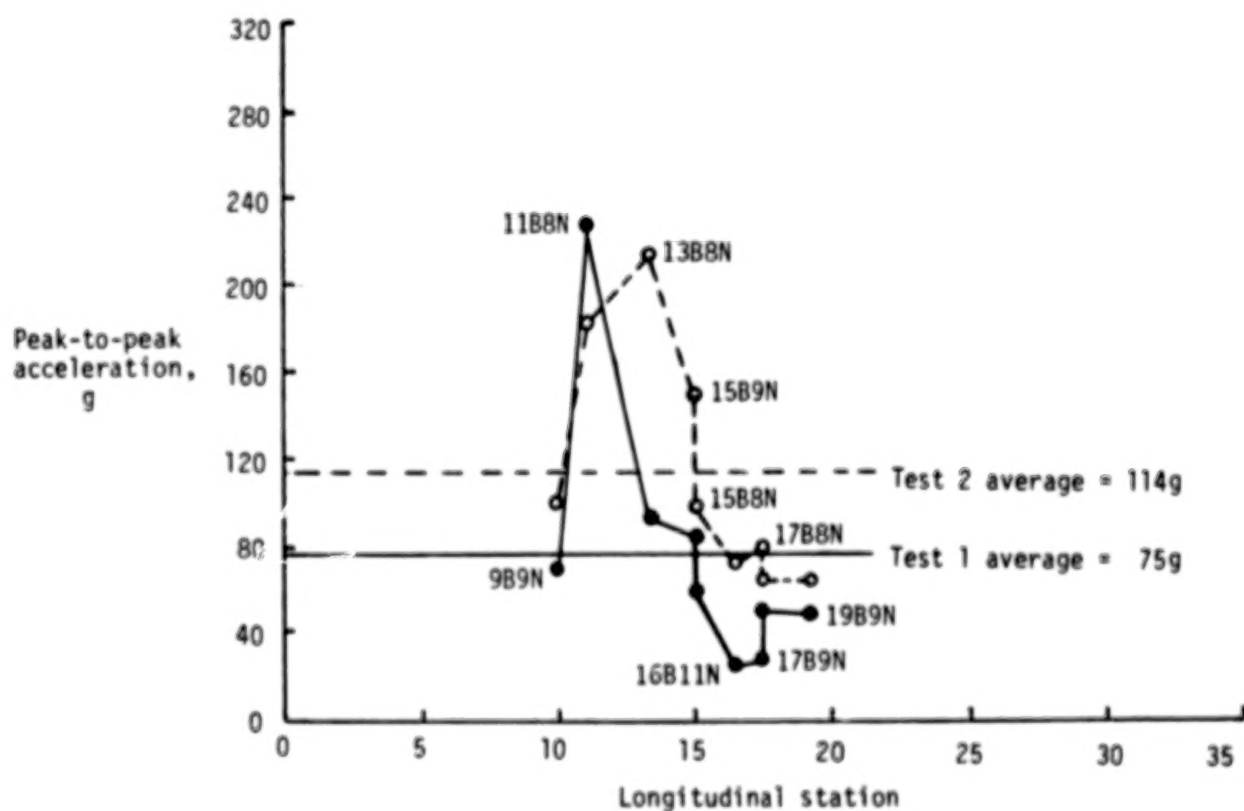
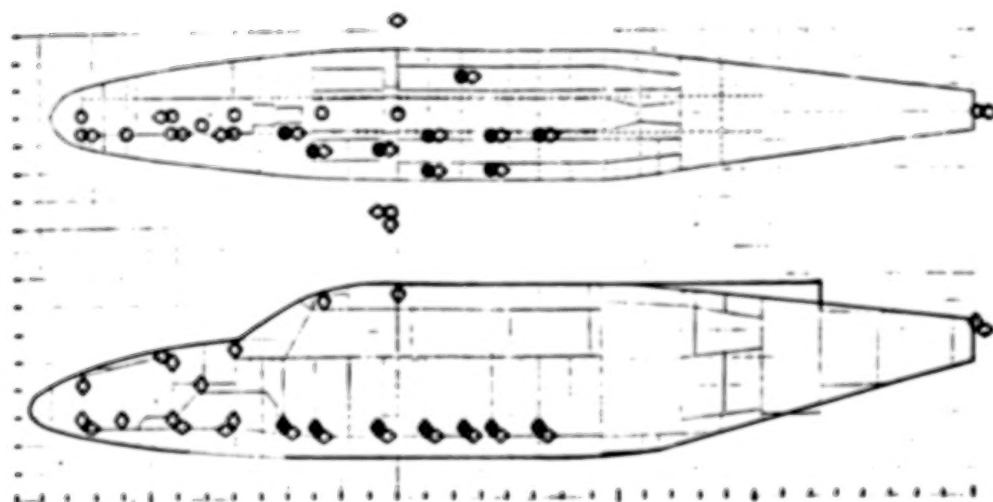
(b) Longitudinal accelerations adjacent to floor beam.

Figure 12.- Continued.



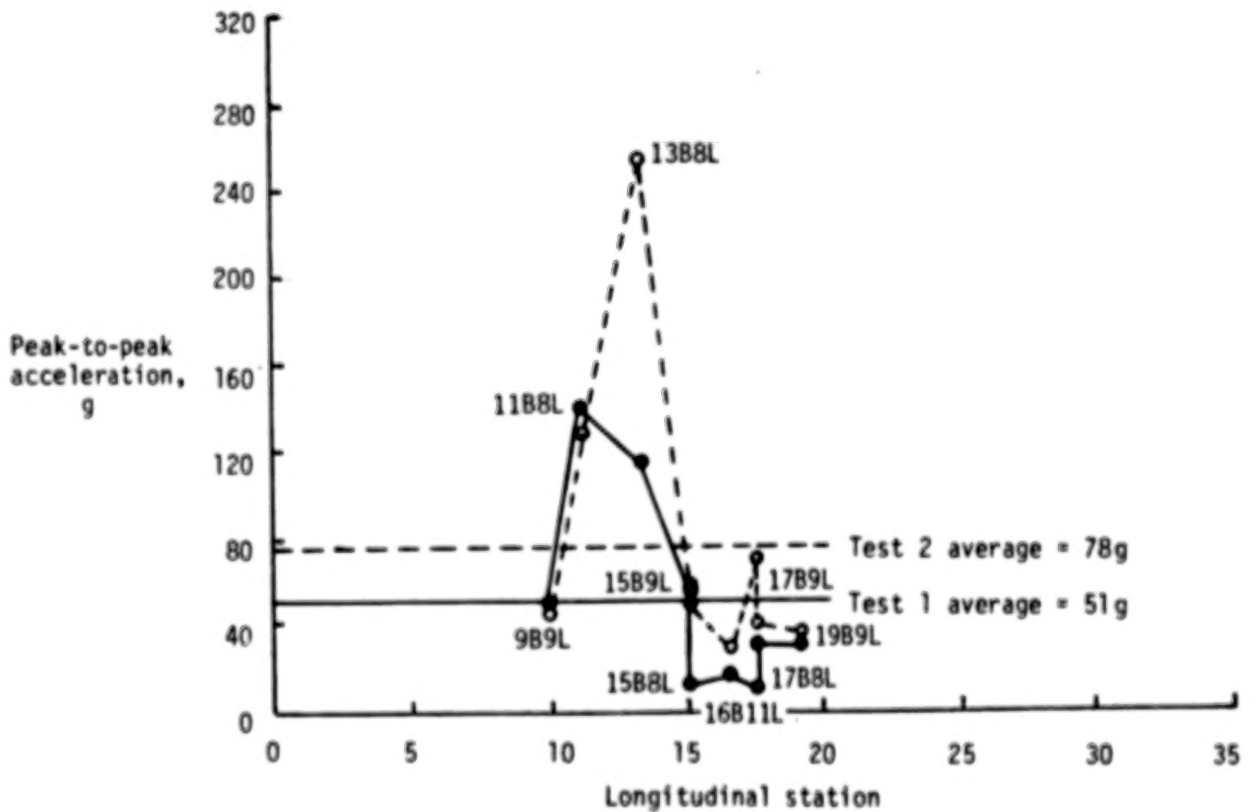
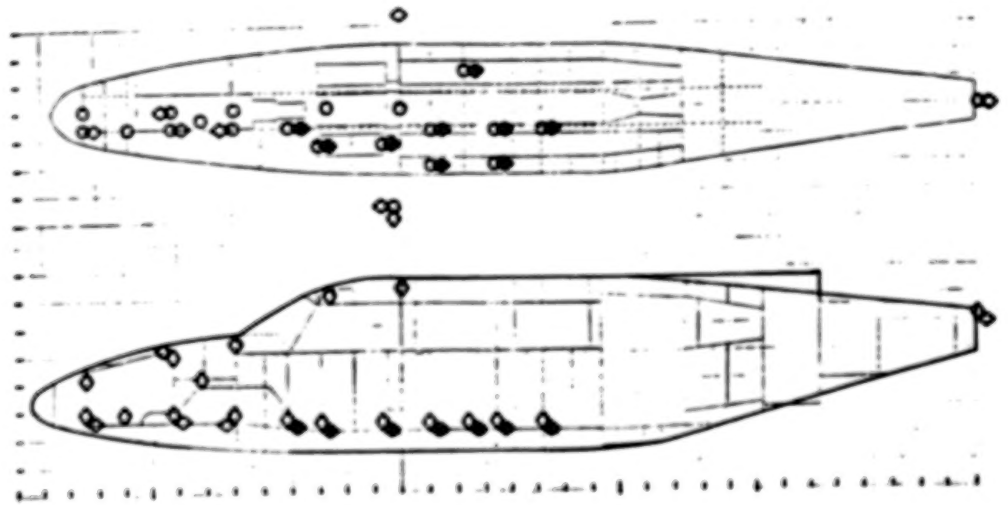
(c) Normal accelerations on roof.

Figure 12.- Continued.



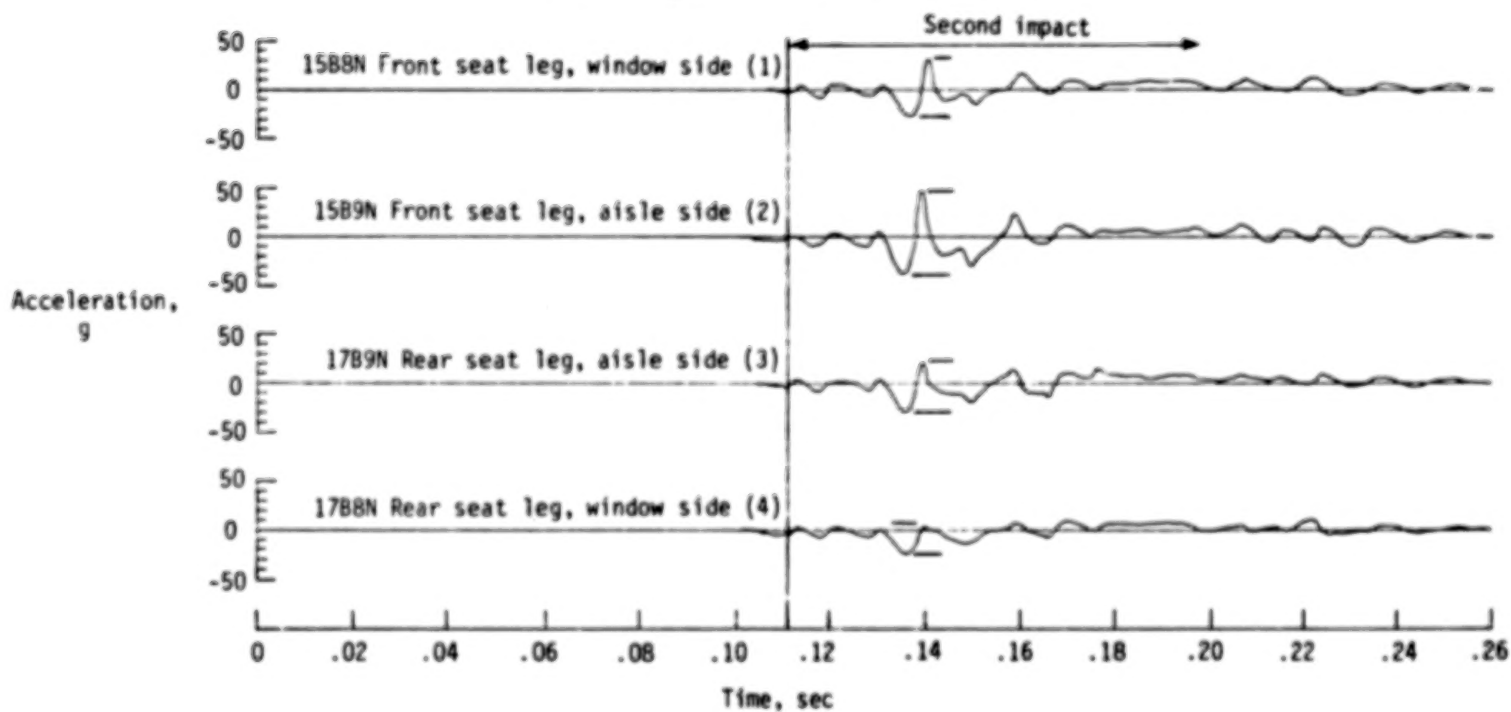
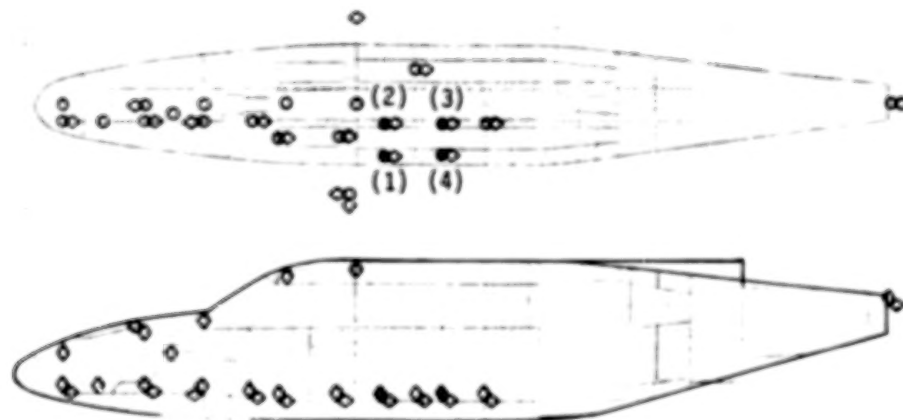
(d) Normal accelerations on cabin floor.

Figure 12.- Continued.



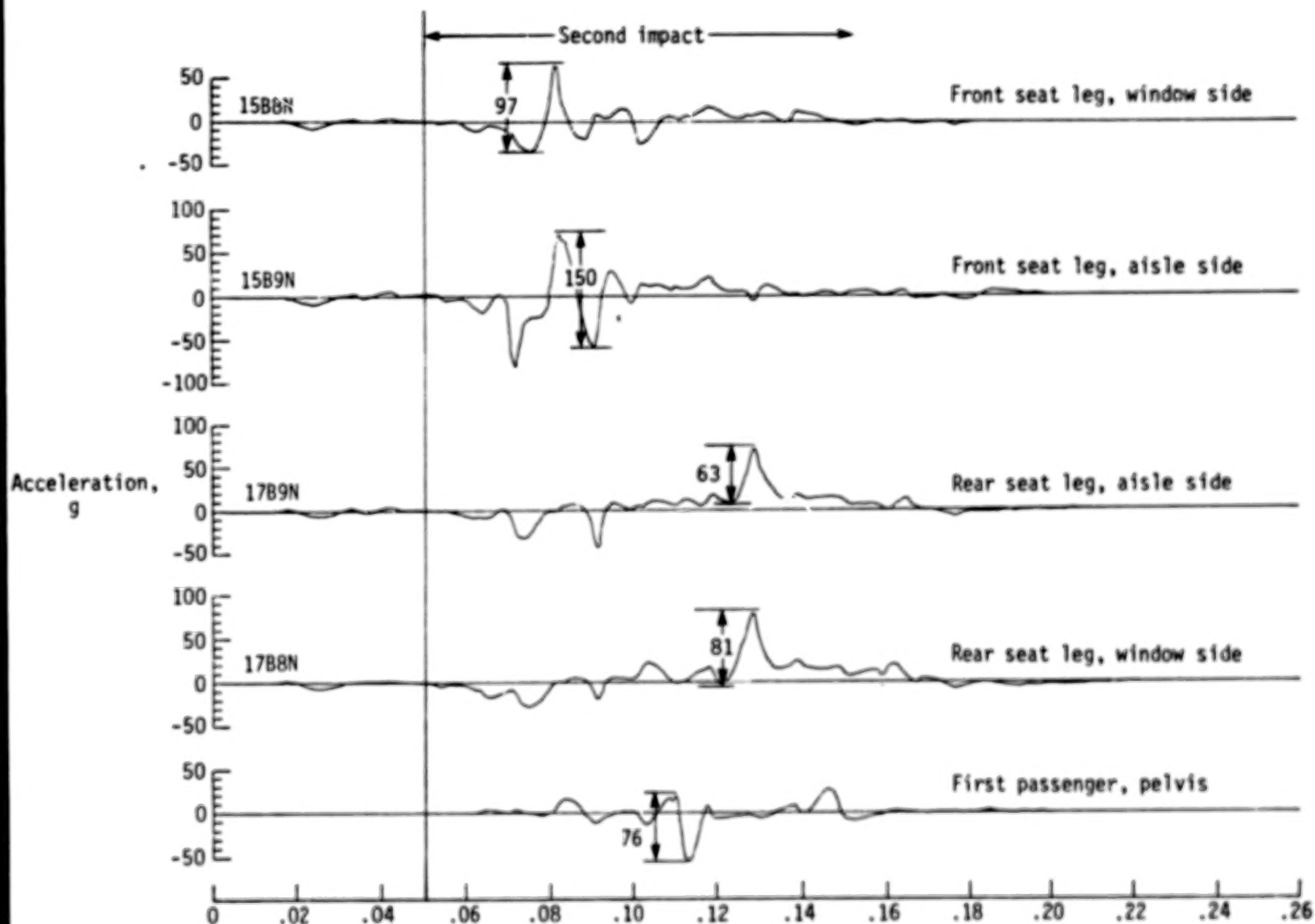
(e) Longitudinal accelerations on cabin floor.

Figure 12.- Concluded.



(a) Test 1.

Figure 13.- Normal accelerations on floor at first passenger seat.



(b) Normal accelerations on floor and dummy pelvis along spine. Test 2.

APPENDIX

ACCELEROMETER DATA

Included in this appendix is the complete set of acceleration time histories for both tests and a schematic to help determine the accelerometer locations corresponding to the time histories. (See figs. A1 to A3.)

The data have been passed through a 4- to 3300-Hz band pass filter during recording, and then digitized at 4000 samples per second. The digitized data were smoothed by a least-squares fit through every 50 points on a third-order polynomial and a 10-point overlap for continuity.

The data are grouped according to the accelerometer location and orientation. The accelerometer location is represented in the schematic by a coordinate system in the x-, z-, and y-directions. The accelerometer normal, longitudinal, and transverse orientations are indicated on the traces by N, L, and T, respectively. Thus, the first accelerometer adjacent to the floor beam in the normal direction is represented by 2B9N. Each station block along the X, Z, and Y axes is 25.4 cm in length.

On the data plots, the abscissa represents elapsed time in seconds. Zero time is the time at initial contact, that is, the time at which the fuselage first contacted the impact surface. The accelerations in the ordinate are expressed in g-units and each trace is identified by the location and orientation of the recording accelerometer.

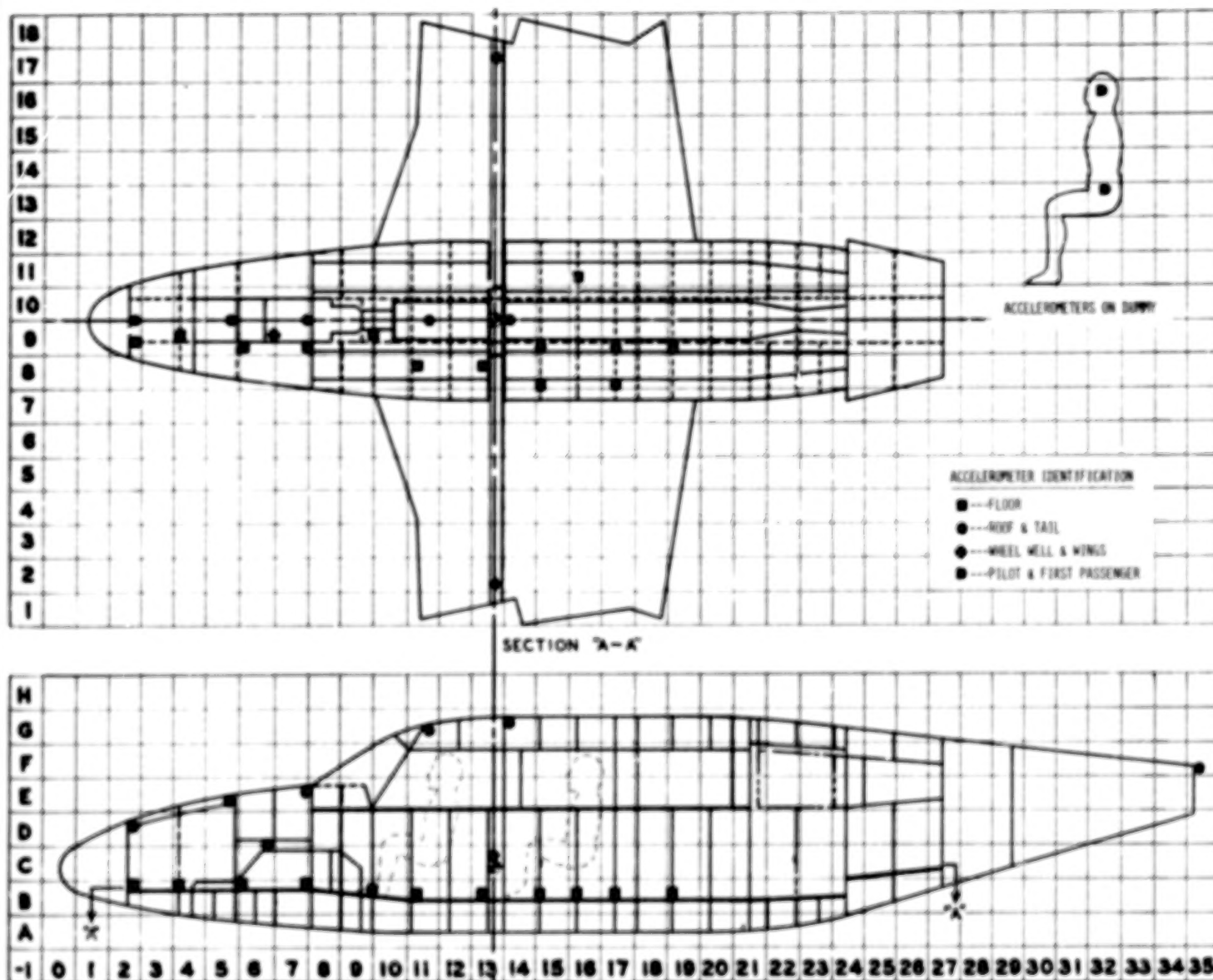
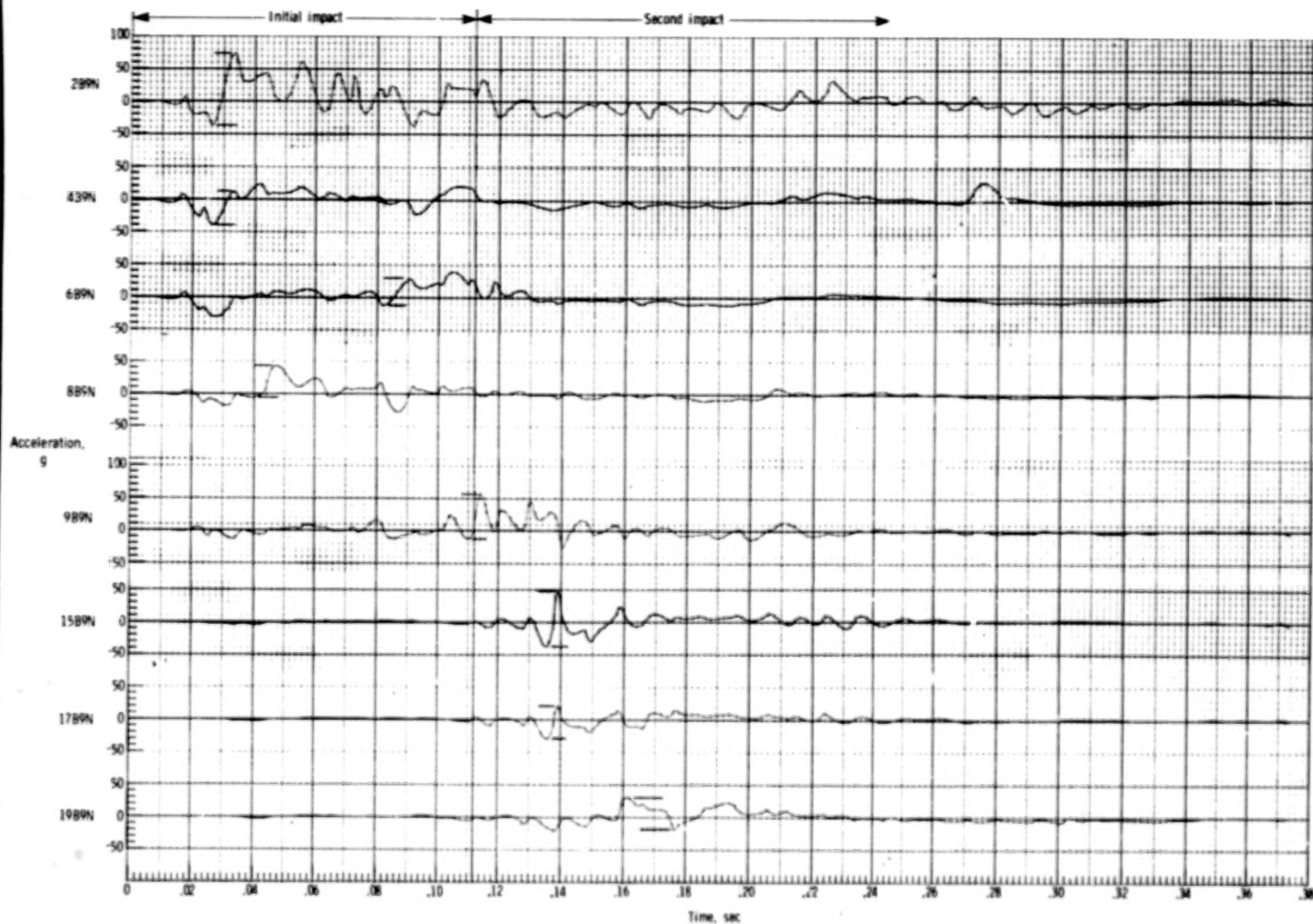
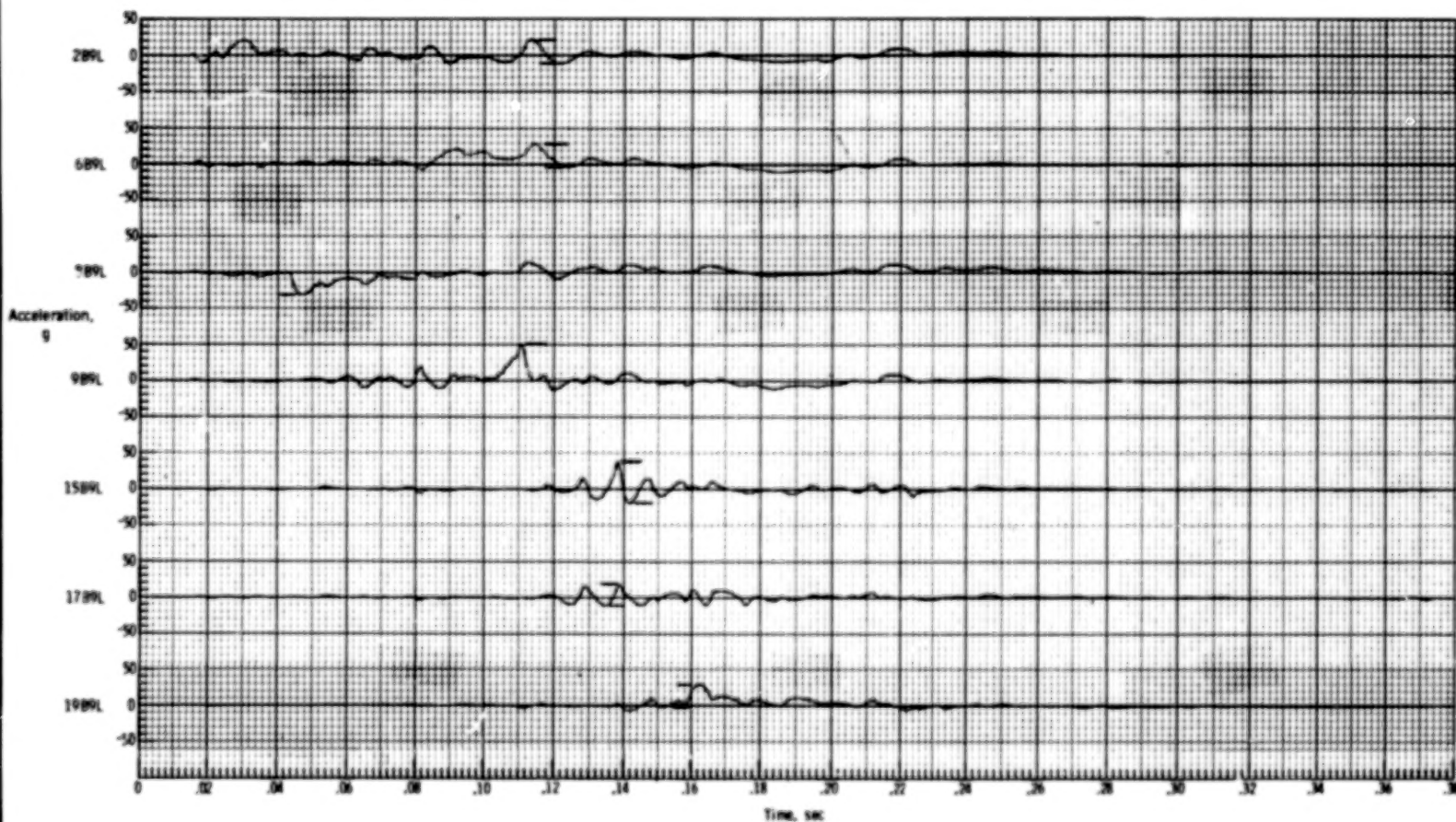


Figure A1.- Accelerometer locations.



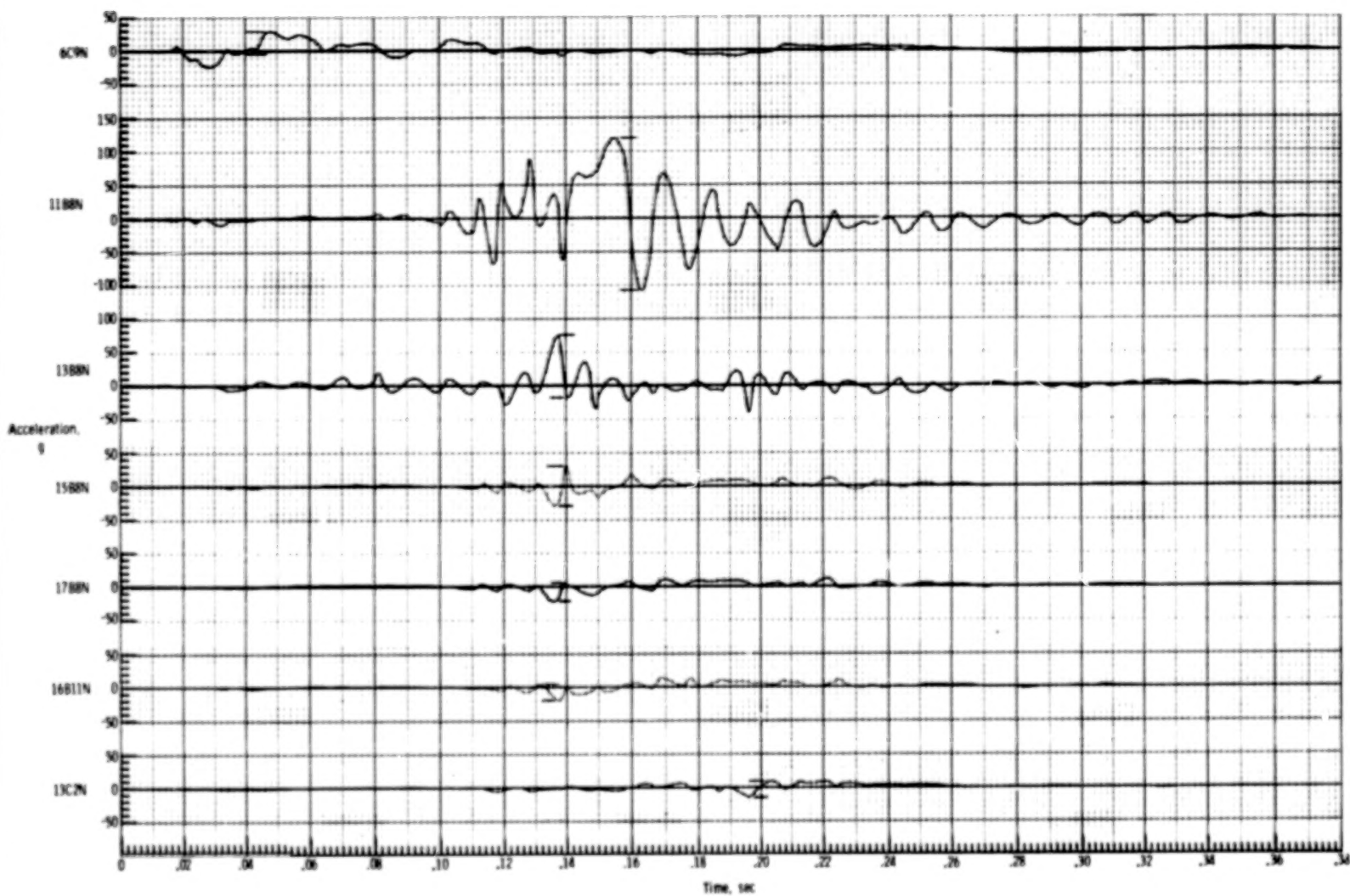
(a) Normal accelerations adjacent to floor beam.

Figure A2.- Acceleration-time histories. Test 1.



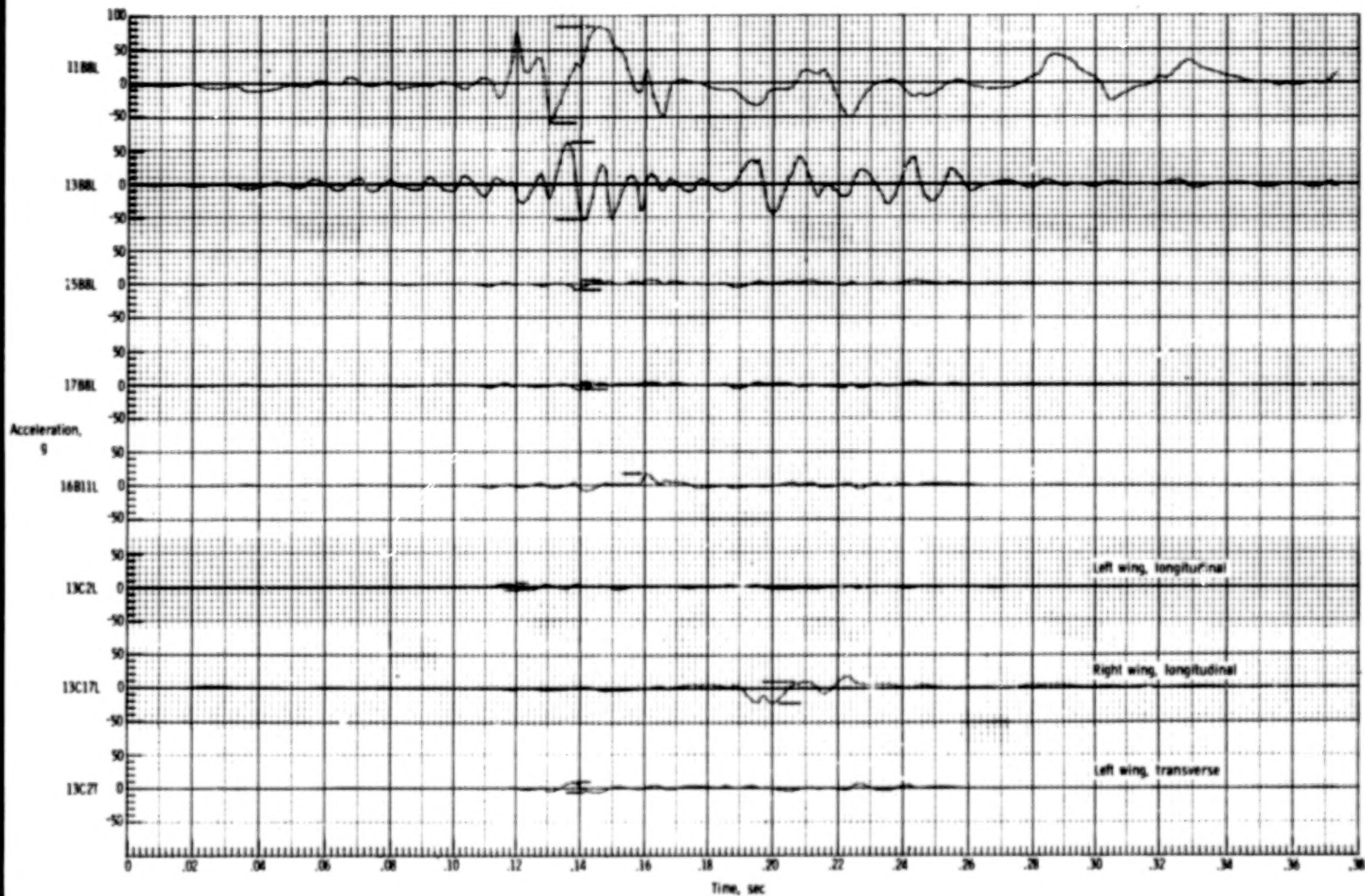
(b) Longitudinal accelerations adjacent to floor beam.

Figure A2.- Continued.



(c) Normal accelerations on cabin floor and wing.

Figure A2.- Continued.



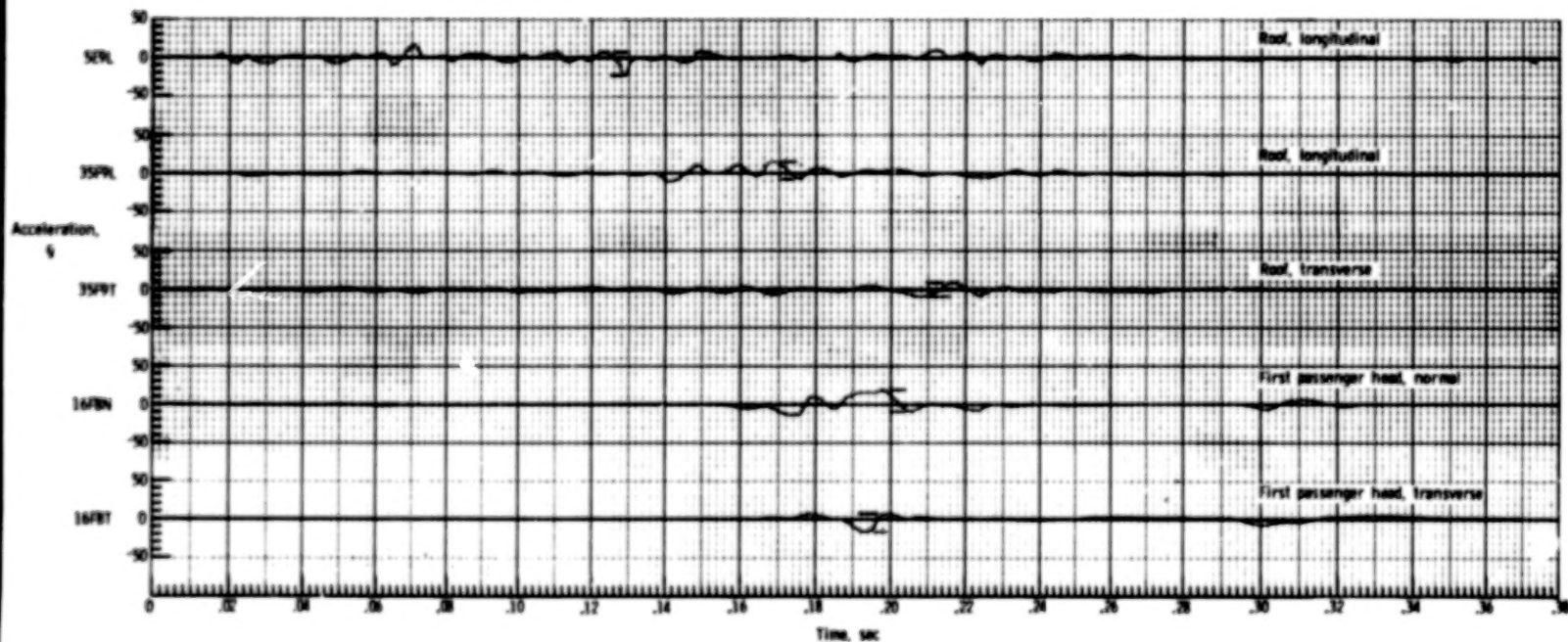
(d) Longitudinal accelerations on cabin floor and wing.

Figure A2.- Continued.



(e) Normal accelerations on roof.

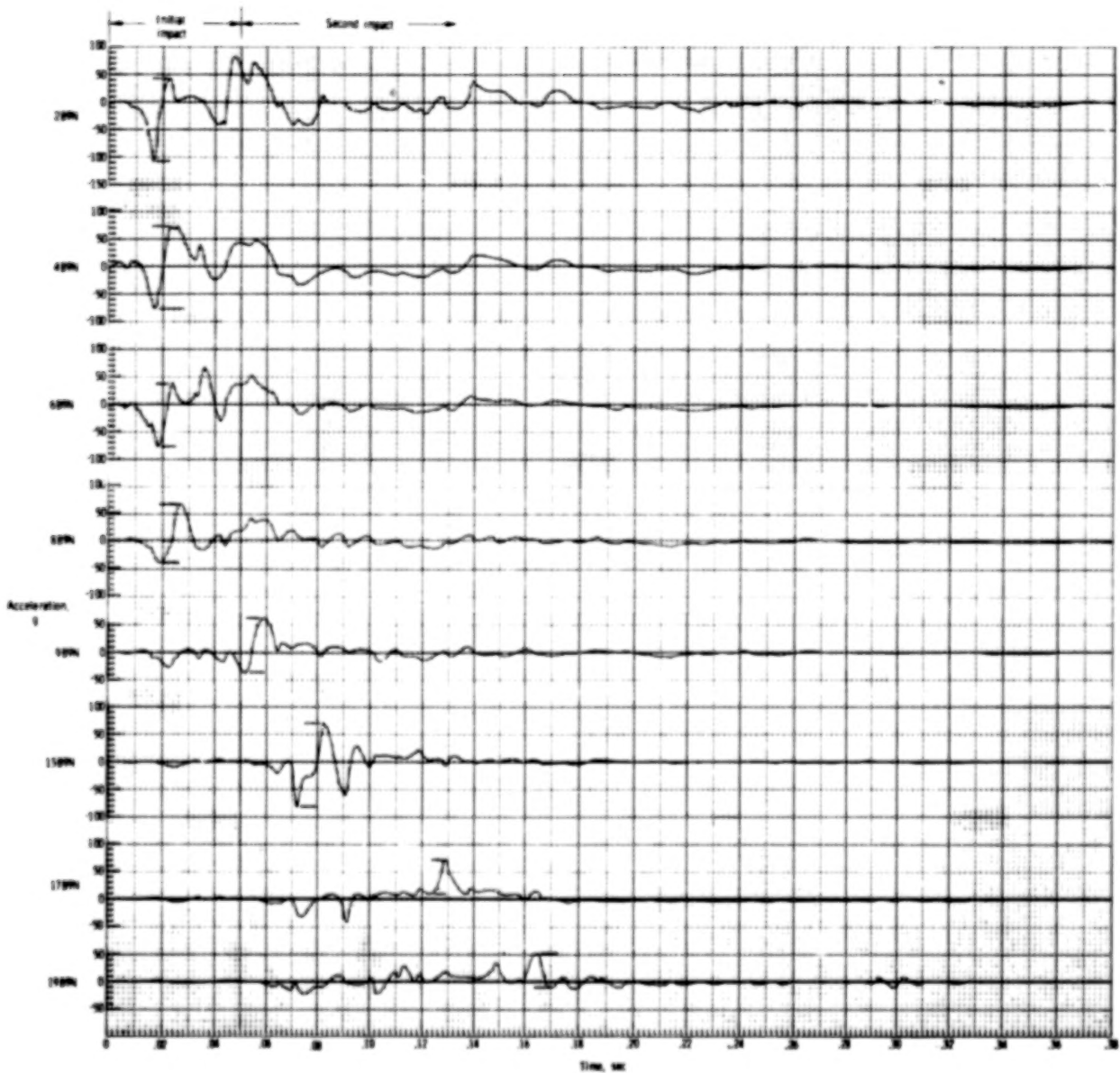
Figure A2.- Continued.



(f) Other accelerations on roof and first passenger.

Figure A2.- Concluded.

APPENDIX



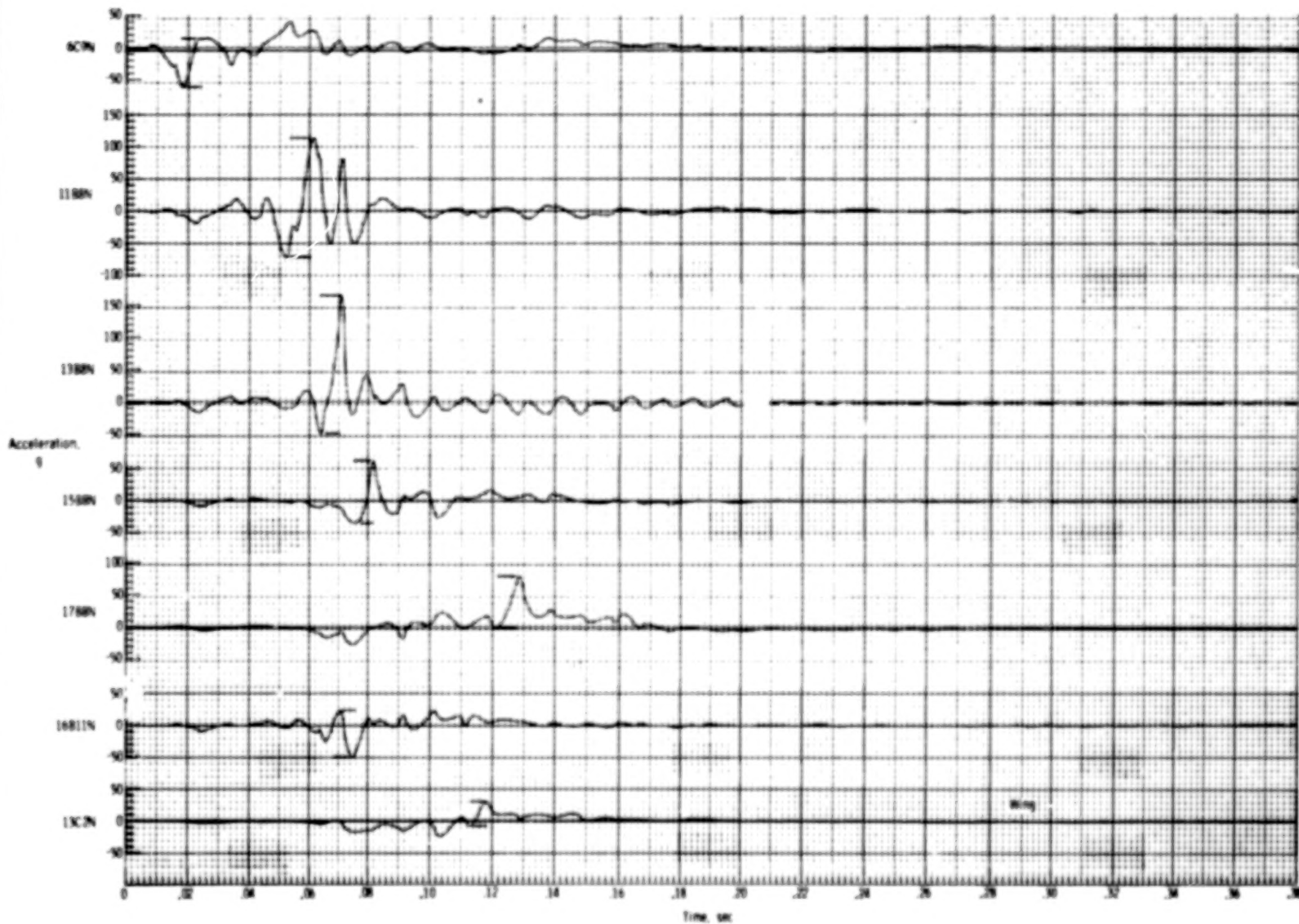
(a) Normal accelerations adjacent to floor beam.

Figure A3.- Acceleration-time histories. Test 2.



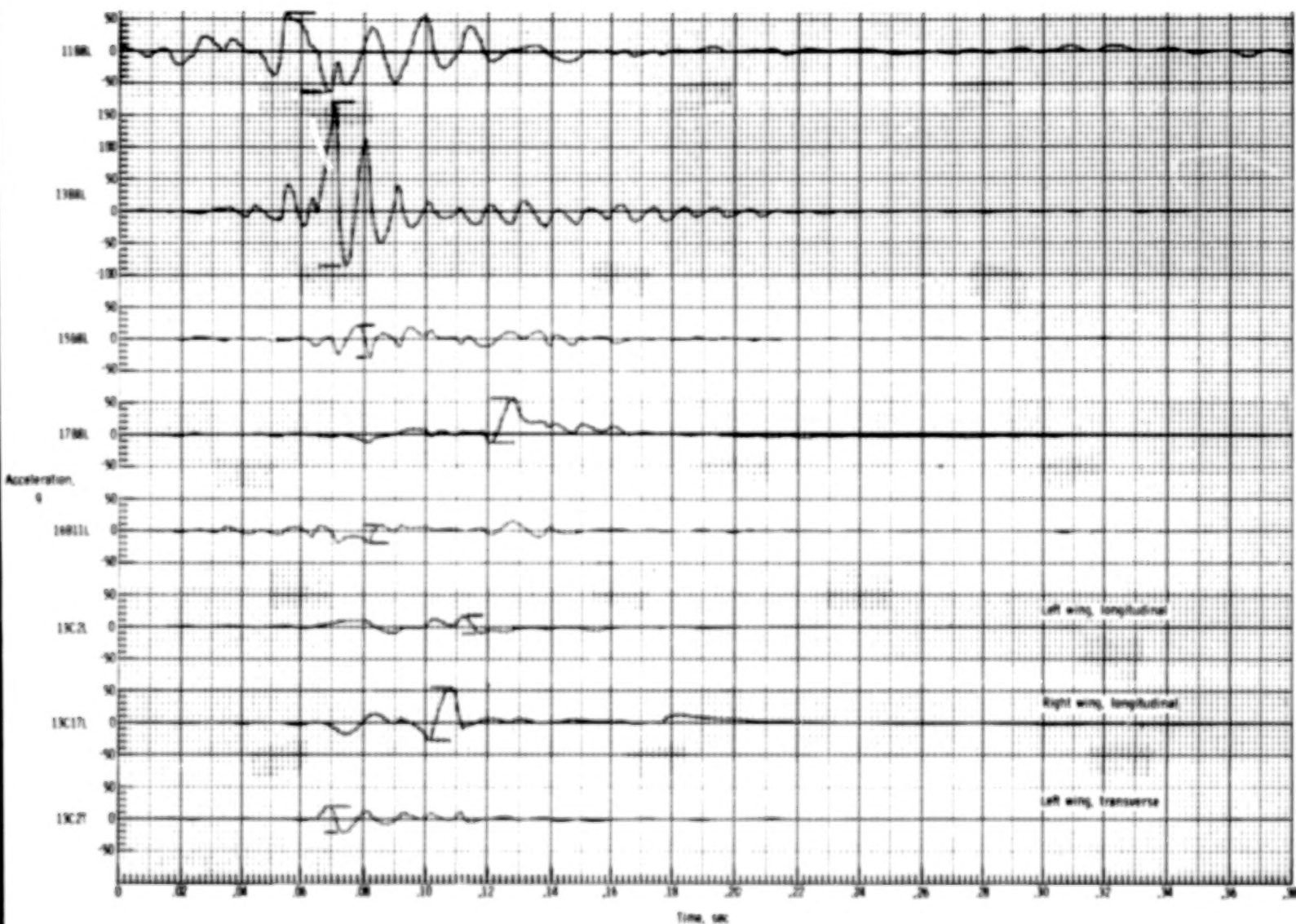
(b) Longitudinal accelerations adjacent to floor beam.

Figure A3.- Continued.



(c) Normal accelerations on cabin floor and wing.

Figure A3.- Continued.



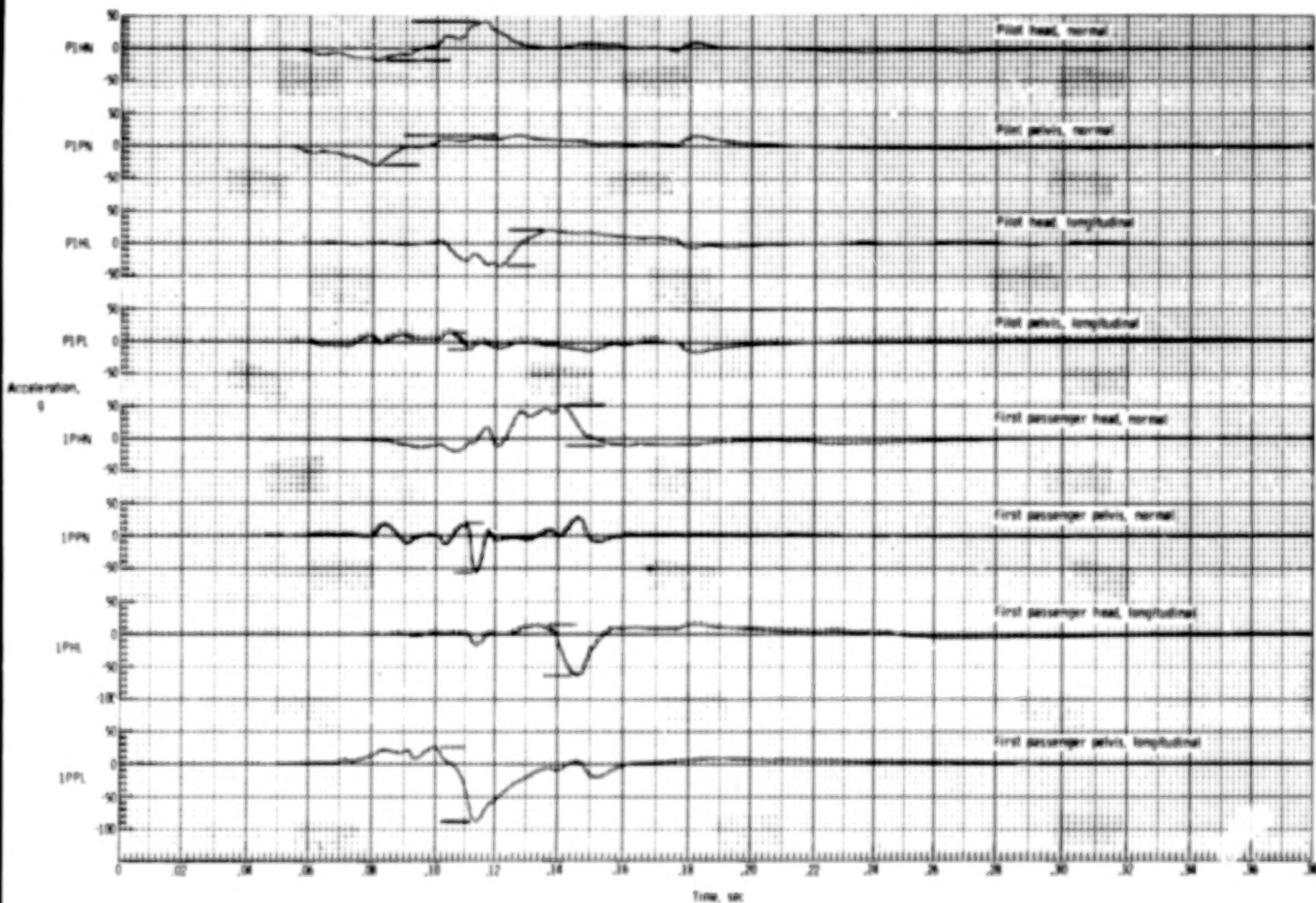
(d) Longitudinal accelerations on cabin floor and other accelerations.

Figure A3.- Continued.



(e) Normal and longitudinal accelerations on roof.

Figure A3.- Continued.



(f) Accelerations of pilot and first passenger.

Figure A3.- Concluded.

1. Report No. NASA TP-1042		2. Government Accession No.		3. Recipient's Catalog No.	
4. Title and Subtitle LIGHT AIRPLANE CRASH TESTS AT IMPACT VELOCITIES OF 13 AND 27 M/SEC				5. Report Date November 1977	
				6. Performing Organization Code	
7. Author(s) Emilio Alfaro-Bou and Victor L. Vaughan, Jr.				8. Performing Organization Report No. L-11426	
9. Performing Organization Name and Address NASA Langley Research Center Hampton, VA 23665				10. Work Unit No. 505-02-13-01	
				11. Contract or Grant No.	
				13. Type of Report and Period Covered Technical Paper	
12. Sponsoring Agency Name and Address National Aeronautics and Space Administration Washington, DC 20546				14. Sponsoring Agency Code	
15. Supplementary Notes					
16. Abstract Two similar general aviation airplanes were crash tested at the Langley impact dynamics research facility at velocities of 13 and 27 m/sec. Other flight parameters were held constant. The facility, instrumentation, test specimens, and test method are briefly described. Structural damage and accelerometer data are discussed.					
17. Key Words (Suggested by Author(s)) Crash worthiness Airplane crash tests Crash damage			18. Distribution Statement Unclassified - Unlimited Subject Category 03		
19. Security Class. (of this report) Unclassified	20. Security Class. (of this page) Unclassified	21. No. of Pages 52	22. Price* \$4.50		